Numerical and experimental investigation of a gasturbine model combustor with axial swirler

Bertsch, Michael

2021

Document Version:
Publisher's PDF, also known as Version of record

Numerical and experimental investigation of a gasturbine model combustor with axial swirler

Numerical and experimental investigation of a gasturbine model combustor with axial swirler

by Michael Bertsch

LUND
UNIVERSITY

Thesis for the degree of Licentiate in Engineering
Thesis advisors: Prof. Xue-Song Bai and Robert-Zoltán Szász, PhD
Faculty opponent: Sven-Inge Möller, PhD

To be presented, with the permission of the Faculty of Engineering of Lund University, for public criticism at https://lu-se.zoom.us/j/68088142340, organised by the Department of Energy Sciences on the 12th of March 2021 at 10:00.

Organization	Document name
LUND UNIVERSITY Department of Energy Sciences Box 118 SE–221 00 LUND Sweden	LICENTIATE DISSERTATION
	Date of disputation 2021-03-12
	Sponsoring organization Swedish Energy Agency through CECOST
Author(s) Michael Bertsch	

Title and subtitle

Numerical and experimental investigation of a gasturbine model combustor with axial swirler

Abstract

This thesis presents the simulations of and experiments with the so-called CECOST burner. The CECOST burner is a gas turbine model combustor equipped with an axial swirler and placed in a laboratory for the lean premixed turbulent combustion of a range of fuels at atmospheric pressure. The operation with natural gas, methane, hydrogen-enriched methane and syngas from black-liquor gasification was investigated experimentally and numerically. The CECOST burner is modular and adaptive, which enables the separate investigation of different parameters. A wide section of the CECOST swirler is manufactured from quartz to enable optical access. The flow field in the combustion chamber was measured by particle image velocimetry (PIV). High-speed imaging of the chemiluminescence signal in the bandwidth of hydroxyl radical relaxation was performed to document the intensity distribution for flames throughout the operating range of the CECOST burner. The lower (lean blow out) and upper (flashback) fuel-air equivalence ratio limits of stable operation were determined. The flashback of the flame upstream into the mixing section was captured by high-speed imaging. In the stable operating range, planar laser-induced fluorescence of hydroxyl radicals (OH-PLIF) was recorded to assess the turbulent flame structure.

Reynolds-averaged Navier-Stokes (RANS) simulations were performed to calculate the steady isothermal flow in the CECOST burner for parameter studies. The measured flow data was used to validate the geometry and numerical discretisation of the computational model of the burner. Large eddy simulation (LES) was carried out to investigate the combusting flow with temporal resolution and high accuracy.

Key words

swirl, burner, gasturbine, LES, methane, hydrogen, flashback

Classification system and/or index terms (if any)

Supplementary bibliographical information	Language
	English
ISSN and key title ISRN: <LUTMDN/TMHP-20/7107-SE> ISSN: <0282-1990>	ISBN 978-91-7895-735-4 (print) 978-91-7895-736-1 (pdf)
Recipient's notes	Number of pages: 67 / Price
	Security classification

Numerical and experimental investigation of a gasturbine model combustor with axial swirler

by Michael Bertsch

LUND
UNIVERSITY

Funding information: The thesis work was financially supported by the Swedish Energy Agency, through the Centre for Combustion Science and Technology, CECOST.

Cover illustration: Flow speed and streamlines in a section of a flow-normal cut plane through the swirler. Predicted by LES of isothermal flow at Re=20,000.

Department of Energy Sciences
Faculty of Engineering
Lund University
Box 118
SE–221 00 LUND
Sweden

ISBN: 978-91-7895-735-4 (print)
ISBN: 978-91-7895-736-1 (pdf)
ISSN: 0282-1990
ISRN: LUTMDN/TMHP-20/7107-SE

Printed in Sweden by Media-Tryck, Lund University, Lund 2021

Contents

List of publications

This thesis is based on the following publications, referred to by their Roman numerals:

I **Flame investigations of a laboratory-scale CECOST swirl burner at atmospheric pressure conditions**

A. A. Subash*, S. Yu, X. Liu, **M. Bertsch**, R.-Z. Szasz, Z. Li, X.-S. Bai, M. Aldén, D. Lörstad
Fuel, Volume 279, 2020, doi.org/10.1016/j.fuel.2020.118421

II **Investigation of turbulent premixed methane/air and hydrogen-enriched methane/air flames in a laboratory-scale gas turbine model combustor**

X. Liu, **M. Bertsch**, A. A. Subash*, S. Yu, R.-Z. Szasz, Z. Li, P. Petersson, X.-S. Bai, M. Aldén, D. Lörstad
In press, International Journal of Hydrogen Energy, https://doi.org/10.1016/j.ijhydene.2021.01.087

III **Numeric investigation of the flame stability for lean premixed combustion of hydrogen-enriched methane and syngas in a lab-scale atmospheric swirl burner**

M. Bertsch, S. Yu, R.-Z. Szasz, X.-S. Bai, A. A. Subash, M. Aldén
Nordic Flame Days 2019, Turku, Finland

Acknowledgements

This work was carried out at the Department of Energy Sciences, Lund University, Sweden. The work has been financially supported by the Centre for Combustion Science and Technology (CECOST).

I would like to express my deep and sincere gratitude to my research supervisors, Prof. Xue-Song Bai and Dr. Robert-Zoltán Szász, for giving me this opportunity to do research and for providing invaluable guidance throughout the project. It was a great privilege and honor to work and study under their guidance. I am very grateful for what they have offered me.

I would like to say thank you to my friends and research colleagues, for their constant encouragement over the years.

Finally, my thanks go to all the people who have supported me to complete the research work.

Popular science summary

Swirl-stabilised flames like the one studied in this project are found in stationary gas turbine engines, often used for electricity generation. In this case, energy is converted from chemical to electric form with a certain efficiency. This efficiency is one parameter to optimise. Another is the emission of pollutants. One step of the conversion between chemical to electric energy is the combustion of fuel with air in the burner unit of the engine, between the compressor and turbine units. It is in this combustor section that a swirl burner can be found. The swirling flame is stabilised aerodynamically, without the need of a mechanic flame holder, which optimises the maintenance cost, another parameter in the design of a gas turbine engine.

The swirl burner studied in this project is a model combustor, this is, it is studies separately, without a compressor and turbine unit. This reduces the complexity and allows to study certain phenomena in detail. For example, the optical access is greatly improved, and advanced laser-diagnostic measurement techniques can be applied. The drawback is that the findings from this model burner can be applied to real, full-scale swirl burners only with limitations.

In this project, an existing model combustor of swirl-flame type was investigated in experiments and modelled with simulation. The experiments aim is to evaluate how the burner behaviour changes when it is operated with fuel gases other than natural gas. Diluting the fuel with for example hydrogen would allow a reduction of the emission of the greenhouse gas carbon dioxide. However, the change of flame behaviour needs to be understood before making design changes towards fuel-flexible gas turbine engines.

The simulations support these experiments where the measurements techniques do not allow to understand the flame behaviour.

Nomenclature

Roman symbols

k	turbulent kinetic energy
p	static pressure
r	radius
S	swirl number
T	temperature
U	velocity
$\overline{U}$	average velocity
U'	velocity deviation
Y	progress variable
y^+	dimensionless wall distance
Z	mixture fraction

Greek symbols

χ	scalar dissipation rate
ε	rate of dissipation of turbulent kinetic energy
μ	dynamic viscosity
ν	kinematic viscosity
ω	specific rate of dissipation of turbulent kinetic energy
ϕ	fuel-to-air equivalence ratio
ρ	density
σ_Z^2	variance of mixture fraction
σ_U	standard deviation of velocity

Subscripts

ax	axial

rad	radial
rms	root mean square
tan	tangential

Acronyms

BL	boundary layer
CECOST	Centre for Combustion Science and Technology
CIVB	combustion-induced vortex breakdown
CL	chemiluminescence
FB	flashback limit
fps	frames per second
GTMC	gas turbine model combustor
IRZ	inner recirculation zone
LBO	lean blow-out limit
LES	large-eddy simulation
ORZ	outer recirculation zone
PIV	particle image velocimetry
PLIF	planar laser-induced fluorescence
RANS	Reynolds-averaged Navier-Stokes
Re	Reynolds number
SGS	subgrid-scale
SST	Menter's shear stress transport

Chapter 1

Introduction

1.1 Motivation

The demand of fuel flexibility for stationary gas turbines is continuously increasing because of the higher cost of conventional fuels and to make accessible new fuel gases from the chemical, petroleum industries, and process industry. Typically these fuels consist of CH_4, H_2, and other light hydrocarbons. Operating engines with these fuels can significantly alter the operation behaviour. State-of-the-art stationary gas turbines are operated under lean and (partially) premixed flame conditions to assure a low pollutant emissions, especially NO_x. Swirling flow is often used to stabilise such a premixed flame aerodynamically. Lean flames are prone to undesired instabilities, such as thermoacoustic oscillations or unsteady flame stabilization [1]. Another risk is for such lean premixed flames is flame blowout at operating conditions close to the lean blow-off (LBO) limit. Due to its high diffusivity and its high laminar burning velocity s_L, fuels containing H_2 are reported to have a lower LBO limit [2–4]. On the other hand, engines operated with these fuels are more prone to flashback [5–7].

It is important when designing and operating a stationary gas turbine engine to have a good understanding of the structures and stability of a turbulent premixed flame, especially in near the flashback and LBO limits. Both undesired phenomena, flashback and LBO, are a result of the interplay between a number of physical and chemical processes. These inlcude, for example, an inner recirculation zone (IRZ) structure following from swirl induced vortex-breakdown [8], which is closely coupled to the gas expansion by combustion [9]. Other factors are finite-rate chemistry effects for a flame near the LBO limit [10], and intrinsic flame instability when H_2 is present in the fuel/air mixture [11]. Computational studies have led to an increased understanding [12, 13], but the relations between the effect of parametric variations [14–16] and combustion limits are still poorly

understood. The stability limits change for each fuel composition, which makes the relations even more complex for dry low emission premixed combustors. In general, the operability ranges become narrower for H_2-enriched CH_4 flames [17, 18]. This thesis presents the findings of experimental and computational investigations of a gas turbine model combustor featuring with a swirl-stabilised flame. This setup is suitable for simulations due to the limited domain extent, and allows optical access in its physical form. Valuable information on the above mentioned relations between a large number of parameters and the operating range limited by flashback and LBO can thus be gained in this research combustor, which can in a second step be applied to design full-scale fuel-flexible industrial stationary gas turbine engines.

1.2 Objectives and scope

The objectives of the here presented study are

(a) to gain an improved understanding of the mechanisms of flame stabilisation, lean blow-off, and flashback of different alternative fuels in gas turbine combustion.

(b) to improve the understanding of the flame structures under stable combustion and close to lean blow-off, as well as close to flashback conditions.

(c) to modify a modular swirl burner for the experimental study and for CFD simulations of alternative fuels under relevant gas turbine combustion conditions.

The scope of this study is as follows:

(a) LES of swirling turbulent flow structures, featuring vortex breakdown.

(b) Experimental measurements of flame stability, and flashback and lean blow-off limits.

(c) Investigation of fuel effects on flame structures under stable combustion and close to the flashback and LBO limits.

1.3 Thesis Structure

Chapter 2 gives an overview and a short introduction into the field of swirl-type turbulent premixed flames. The literature on relevant swirl-type gas turbine model combustors is presented. Following the presentation of experimental work

in this field, Chapter 3 gives a summary of selected numerical investigations of swirl-type research combustors that are reported in the literature. This is followed by Chapter 4 that presents the CECOST swirl burner, the setup on which the here presented experimental and numerical investigation are based on. After the setup description, Chapter 5 presents and discusses selected new results from the study of the CECOST swirl burner. This chapter is to be seen as a complement to the findings presented in Papers I-III. This means the focus is on experimental and numeric material that is not mentioned explicitly in these publications, which are summarised in Chapter 6 and can be found in the Appendix of this thesis in full-length. Finally, Chapter 7 gives a brief summary of the presented conclusions and suggestions for future work with the CECOST swirl burner.

Chapter 2

Swirling turbulent premixed flames

2.1 Vortex breakdown and flame stabilization in turbulent swirl premixed flame

In this section, the physical mechanism of vortex breakdown in turbulent swirl premixed flame (TSPF) will be discussed. Swirling flows are widely encountered in aircraft wingtip vortices, some heat exchanger designs, cyclone separators, and modern low emission gas turbine engines. Before studying the interaction of vortex breakdown and turbulent swirl premixed flame (TSPF), the structures of vortex breakdown and premixed flame should be investigated separately at first. Taamallah et al. [19] describe two types of structures that exist in swirling flow:

- Kelvin-Helmholtz instability induced structures: In swirling flows, the combined axial-azimuthal shear layer gives rise to a helical vortex that winds around the shear layer.
- Helical instability-induced structures: above a certain swirl strength, the inner swirling core can develop self-sustained oscillations and transitions to a limit cycle regime following a supercritical Hopf bifurcation.

Several different flame macrostructures have been reported in swirl-stabilized combustion. These have been previously documented as functions of several parameters such as the fuel composition, equivalence ratio and preheat temperature, and Reynolds number, swirl number and confinement as well as centerbody geometry. Chterev & Seitzmann [20] list the following flame macrostructures: a columnar tubular flame (I); a bubble-columnar flame (II); a single conical flame stabilized along the inner shear layer ISL (flame III); and a double conical flame

with an additional flame front stabilized in the ORZ and along the outer shear layer OSL (flame IV) [20]. They describe the interaction of vortex breakdown and flame as follows:

- Vortex breakdown affects the mixing process between the fuel, air, and hot combustion products and thereby affects the heat release rate.
- Vortex breakdown wrinkles and stretches the flame.
- Reactivity and the heat release rate can be enhanced (positive stretch with Le <1) or reduced by vortex breakdown.
- Heat release and thermal expansion and baroclinic vorticity can affect the vortex structure

Physical Mechanism

A study by Taamallah et al. [21] reports that with the equivalence ratio of a swirling flame increasing, a transition will happen from flame (I) to flame (IV). After the transition to flame IV, the turbulent flame becomes on average more intense due to the increased heat release at higher equivalence ratio [21]. The flame becomes also more compact; a shorter flame is due to the higher burning velocity requiring lower flame surface area. It is also due to the creation of a new flame surface around the ORZ. A slight change in incoming flow angle is observed; this can be attributed to the thermal expansion of the ORZ when the flame appears there as this zone becomes recirculating combustion products instead of reactants. Moreover the interrogation of the flow field highlights the change in the IRZ structure when the transition takes place. Flame III means that the flow field shows a lobe shaped IRZ that can also be noticed from the associated chemiluminescence image. This lobed structure, having a region of positive velocity along the IRZ's centreline, disappears when the flame becomes established in the ORZ [21].

2.1.1 Flashback

Flashback is an intrinsic behaviour of premixed combustion systems and it can occur where fuel and oxidizer are already mixed upstream the flame front. Several explanations of flashback can be found in literature but none of them are universal [22]. Flashback occurs when auto-ignition takes place in the mixing zone [23] or the flow velocity and the flame speed are similar each other. Flashback occurs due to several possible mechanisms:

- Flashback by autoignition:
  Autoignition occurs when the gas residence time exceeds the reactant

mixture ignition delay time, leading to the ignition of the mixture in the mixing zone. This phenomenon is strongly influenced by local temperature, pressure and equivalence ratio [24].

- Flashback in boundary layers:
  In boundary layers, the velocity is sufficiently low to allow upstream propagation of the flame, even though it is limited by wall quenching. One of the most widely used models is the one proposed by Lewis and von Elbe as mentioned in the review of Plee & Mellor [23] in which the wall velocity gradient and the ratio of the laminar flame speed S_L over quenching distance d_q determine whether a boundary layer flashback event occurs.

- Turbulent flame propagation in the core flow:
  This propagation is possible when the turbulent flame velocity S_T becomes higher than the local flow velocity. Such a situation can occur in swirling flames, where turbulence is intense.

- Combustion instabilities leading to flashback:
  Combustion instabilities are due to a coupling between heat release, pressure fluctuations and flow hydrodynamics. Velocity fluctuations induced by instabilities can be huge enough to be comparable to the mean flow velocity and lead to a transient flashback during the oscillation cycle [25].

- Flashback induced by vortex breakdown: Various mechanisms control the behaviour of swirling flows and one of them is the vortex breakdown [26]. It can be defined as an abrupt change in the jet topology and can take several forms [27].

2.1.2 Lean blow-off

In this section, the lean blow-off is investigated with a focus on the turbulent swirling premixed flame, which are commonly used in gas turbine engines. The blow-off happens generally when the flow speed becomes much higher than the flame burning velocity, and the flame front is convected downstream with the flow. Therefore, the fresh unburnt mixture will not be ignited and the flame will be extinguished. This phenomenon is extremely important in modern gas turbine engines because they are operated in the lean premixed regime, close to the lean blow-off (LBO) limit.

In a gas turbine engine, a high turbine inlet temperature is desired to increase the overall engine efficiency. By the recent advances in the material production

and the cooling methods, a first law efficiency of up to 60% can be obtained increasing this temperature from around 1500°C to 1600°C [28]. However, this high temperature, leads to high amounts of NO production and emission.

In order to reduce the amount of NO emissions from an engine, several methods such as fuel staging, inert species dilution, and exhaust gas cleanup are available [28]. Nevertheless, all of these methods would increase the capital or running cost of the engine, or reduce its overall efficiency. Another method which is commonly applied to reduce the NO emissions from the gas turbine engines, is the combustion in the lean premixed regime. In this regime, by reducing the equivalence ratio, the maximum temperature in the combustion chamber and hence the NO emissions will be reduced. However, there are challenges with lean premixed combustion as well. Two major problems with this method are the CO emissions and the combustion stability, which should be further studied [28]. Another factor, which makes these studies even more complex, is the fact that syngas (a mixture of mainly CH_4, CO, and CO_2) is commonly used as fuel in gas turbines. So the fuel composition can be different in each case and it should be considered in all studies.

In the following two subsections of this chapter, the mechanism of blow-off will be investigated first. A simple laminar bluff-body stabilized flame from the literature is presented to learn more about blow-off mechanism. Then on the next subsection, the various parameters which are effective on the blow-off are summarized.

2.1.3 Blow-off mechanism

Kedia & Ghoniem [29] numerically investigate the blow-off mechanism of a bluff-body stabilized premixed flame. They perform two-dimensional simulations with a detailed kinetic mechanism. The LBO limit is approached by reducing the equivalence ratio in the simulations and they investigate the location and the conditions at which blow-off occurs. This subsection is mainly a summary of their work, which is helpful for understanding the blow-off mechanism.

In order to have a stable flame, two conditions should be satisfied. First, the flame displacement speed should be equal to flow speed. And second, the gradient of flame displacement speed normal to flame surface should be higher than the gradient of the flow speed on the same direction. These two conditions can be expressed as

$$|S| = |U_n| \tag{2.1}$$

and

$$\left|\frac{dS}{dn}\right| > \left|\frac{dU_n}{dn}\right|, \tag{2.2}$$

where S is the flame displacement speed, U_n is the flow speed normal to the flame surface, and n is the direction normal to the flame surface [29]. The first equation is the static stability condition and if satisfied the flame will remain in its place. The second condition is the dynamic stability criterion. If this second condition is satisfied, a minor perturbation cannot grow and change the location of the flame front. For instance, at position n_0 the flame is stable and the flame displacement speed is equal to the flow speed. If any perturbation cause the flame to move toward the n direction (toward reactants), the flame displacement speed will be lower than the flow speed in the new location. Therefore, the flow will move the flame back to its position. On the other hand, if the flame is somehow moved toward the products (opposite of n direction), the flame displacement speed will be higher than the flow speed, and the flame propagates to its previous location [29].

If the dynamic stability criterion (Eq. 2.2) is not satisfied, any perturbation can cause a disturbation of the flame and there is no mechanism to return the flame front to its original place. In the 2-D numerical simulation of a bluff body stabilized flame presented by Kedia and Ghoneim [29], it has been observed that for low equivalence ratios, ϕ, lean blow-off starts downstream of the recirculation zone, where the dynamic stability condition is not satisfied (Eq. 2.2). At that location a distinct flame pinch-off is observed, dividing the flame into two parts. One part of the flame (downstream of the recirculation zone) is moved with the flow toward the domain outlet. The other part which is inside the recirculation zone remains in the domain for several milliseconds, which is called the residual flame. The residual flame is also extinguished after a short while and there will be no more flame due to blow-off.

In order to calculate the $|dS/dn|$, the equation

$$\left|\frac{dS}{dn}\right| = \left|\frac{dS}{d\kappa} \times \frac{d\kappa}{dn}\right| \tag{2.3}$$

where κ is the total flame stretch. In this equation, $d\kappa/dn$ is a property of the flow which can be measured from the simulation data. Furthermore, $dS/d\kappa$ is a physio-chemical property of the reacting mixture and for small values of flame stretch, is equal to the negative value of the Markstein length [29].

In a more recent study, Rock et al. [30] investigate the near blow-off dynamics in a liquid fueled combustor. Even if this study is not focused on premixed flame, some features are similar in spray flames or premixed flames. They have indicated that there are reasonable correlations available for prediction of the LBO limit, but the dynamics of this phenomenon is not very well known. The blow-off process happens in two stages, starting with the local extinction of reactions, followed by large scale changes in the flame and flow dynamics. They have investigated the near blow-off dynamics for 10 different fuel types and two

different inlet temperatures to investigate the important phenomena such as extinction, ignition and recovery of the flame. They have observed that in near LBO limit, the recovery mainly happens because of the convection of hot gases to upstream, and partly because of the flame propagating upstream. Furthermore, they have argued that the extinction events are mainly due to the convection of the flame to the downstream of the flow [30].

Morales et al. [31] also investigated the mechanisms of LBO for a bluff body stabilized flame, using simultaneous PIV and CH* chemiluminescence. They have observed that the flame-vortex dynamics (reduction of flame-generated vorticity coupled with decrease in downstream shear layer vorticity) are the main driving mechanism of flame extinction [31].

CFD simulation is a strong tool to study the mechanisms of blow-off. Especially, with the recent advancement in numerical methods and hardware developments, LES (Large Eddy Simulation) became more and more popular to study the combustion in different engines with highly accurate results. For instance, Giusti & Mastorakos [32] performed an LES simulation coupled with Conditional Moment Closure (CMC) combustion model for a swirling ethanol spray flame. Their main objectives are to further validate the capability of LES/CMC in prediction of local extinction, and also to study the mechanisms leading to the local extinction. Hodzic et al. [33] performed an LES simulation of a bluff-body stabilized premixed flame close to LBO conditions. It is found that local extinction in shear layer has only a minor impact on blow-off. The blow-off in their case was mainly attributed to the flame migrating to the recirculation zone and the series of events that happens afterwards.

2.2 Effects of parameters on lean blow-off

Knowing the criteria for stable flame and lean blow-off, it can be easily concluded that any variable which affects the flame velocity, or the flow velocity, can also change the lean blow-off (LBO) equivalence ratio. The following parameters from the literature are some of the most important factors affecting the LBO limit:

- Bulk axial velocity
- Fuel composition
- Water addition
- Dilution in inert species

In the following, some of the recent publications on the above mentioned parameters and their effects on LBO limit will be discussed. The main focus is

on the turbulent swirling premixed flames. Therefore, the recent publications focused on this type of flames are analysed. Such papers for each parameter mentioned above, and in that case, other flame types are also considered.

2.2.1 Bulk axial velocity

Schefer et al. [34] performed experimental investigation of the flame instability and LBO limit for hydrogen-enriched methane air flames. In their experiments, they have used a swirl-stabilized burner and changed the reactant flow rate until instability and blow-off observed. They have defined the flame instability as a state of weakening of the flame anchoring, which produces a tornado-shaped flame in the center of the combustor [34].

They perform several experiments with various amounts of H_2 enrichment to measure the LBO limit against reactant flow rate. They conclude that by increasing the reactant flow rate (or bulk axial velocity) the equivalence ratio of lean blow-off, ϕ_{LBO} will be higher. It means that by reducing the reactant flow rate, the flame will be more stable at lean conditions. In other words, by moving toward more lean mixtures, the laminar burning velocity is lower and hence the blow-off can happen at a lower flow velocity [34].

Furthermore they investigate the effect of hydrogen enrichment on lean blow-off. It is found that hydrogen addition makes the flame stronger and lowers ϕ_{LBO}. It is also demonstrated that hydrogen enrichment greatly reduces the CO emissions while has minor effects on NO emissions [34].

2.2.2 Fuel composition

As it was mentioned earlier, syngas is a promising fuel to be used in gas turbines for power generation. Since syngas fuel can be any mixture of CH_4, H_2 and CO, the effects of fuel mixture on the LBO should be investigated precisely. Zhang et al. [35] measured the LBO limits for several different mixtures of CCH_4, H_2 and CO. They indicated that one of the basic difficulties for investigation of LBO limit is the fact that the mechanism of blow-off is different for different fuel mixtures. For instance, for low amounts of H_2 in the fuel mixture, the blow-off happens abruptly with a slight change in fuel composition. However, for mixtures with more than 50% or more H_2, they have observed distinct flame lift-off prior to flame blow-off. Therefore, they have defined the blow-off in their experiments as the point where no flame can be observed in the optical accessible part of their combustion chamber.

Oztarlik et al. [36] also investigated the effects of fuel composition on the instability of the turbulent premixed swirling flame. They experimentally investigated the effects of addition of H_2 to the CH_4-air mixture, or adding hydrogen or

methane as pilot fuel. They observed that even small values of hydrogen as pilot fuel can significantly increase the stability of the lean flame. However, adding the same amount of hydrogen to the fuel-air mixture, has no significant effect on flame stability and LBO limit. Adding methane as pilot fuel is also effective but it is less significant. The other important factor that has to be considered in case of using pilot fuel, is the emissions from the burner. In this research, they have observed that adding pilot fuel has no significant effect on CO emissions, but it increases the NO emissions considerably.

In another related study, Han et al. [37] used both experimental and numerical studies to investigate the interactions between the pilot and main flames. Three different conditions i.e. only pilot flame, only the main flame, and the stratified flame with both pilot and main flame are investigated. In the case of V-shaped pilot flame, they have observed that by increasing the air flow (through the main inlet), the flame will move toward M-shaped flame and it will be less stable because the fuel is diluted in the surrounding air. In the second case, the flame will be lifted if air is supplied through the pilot inlet and the temperature of the main recirculation zone will be lower.

2.2.3 Water addition

Another interesting parameter which affects the LBO limit and emissions of a premixed flame is the water content of the mixture. Pugh et al. [38] investigated the effects of H_2O vapour/spray on lean blow-off and emissions in a premixed turbulent swirling flame. It has been argued that H_2O has catalytic effects on highly carbonaceus syngas mixtures. Therefore, small amounts of water vapour can increase the laminar flame speed and reduce the LBO stability limit. However, by increasing the amount of water, the fuel mixture will be diluted which results in a lower adiabatic flame temperature and a slower reaction.

2.2.4 Dilution with inert species

Dilution of fuel-air mixture is one of the important effective parameters on LBO limit of a premixed flame. It has been argued that dilution affects the flame in at least four ways: (1) mixture heat capacity, (2) transport properties, (3) chemical kinetics, and (4) radiative heat transfer [39]. Marsh et al. [40] investigated the operating limits of premixed methane oxycombustion in N_2 and CO_2 atmospheres. It has been observed that CO_2 dilution has a more significant impact on flame location, heat release, and operation response, compared to N_2 environment. Furthermore, combustion in CO_2 environment increases CO emissions, but it is argued that it is mainly attributed to the lower flame temperature, rather

than thermal dissociation. On the other hand, combustion in N_2 environment increases the NO emissions.

2.3 Thermo-acoustic instability

A review of the stability of lean premixed swirling flames is reviewed by Huang & Yang [41]. They name two fundamental causes for instabilities in combustion chambers:

- Combustion chambers are lined by walls and the internal processes attenuating unsteady motions are weak.
- The heat released by combustion represents a very small fraction of the energy required to drive unsteady motions.

Lean-premixed combustion systems are especially prone to flow oscillations for several reasons:

- The system often operates near the lean blowout limit. A small perturbation of the equivalence ratio (ϕ) can lead to a large variation in heat release. The heat release fluctuation, if in resonance with a chamber acoustic wave, can lead to large-amplitude combustion oscillations.
- Different to diffusion-flame type combustors, little dilution or film cooling air is injected along the combustion chamber wall. The diluting air supply would act as an efficient acoustic damper to suppress resonant amplification of combustion oscillations.
- In premixed combustors for power generation the flame is typically short compared to the combustor's longitudinal acoustic wave length, and the flame is in most cases situated at the acoustic pressure anti-node point. This acoustically compact configuration facilitates the interactions between oscillation of heat release and flow motion.
- As the flame is typically stabilised by aerodynamically induced recirculating flow, a high-amplitude flow oscillation can cause flow reversal and even flame flashback into the mixing section.

It is still a challenge to simulate thermo-acoustic instability in gas turbine engines owing to the multi-scale physics problem. Rather few numerical simulations have been presented in the recent literature. Among the few papers, Chen et al. [42] successfully capture the experimentally observed effect of thermo-acoustic oscillation on the precessing vortex core (PVC) by compressible LES of an unstable premixed dual-swirl flame. Spalding's wall formula is applied

to model near-wall turbulence, and laminar uniform inlet velocity profiles are specified at the inlets. An extended farfield domain is added with atmospheric pressure outlet boundary condition.

2.4 Syngas combustion in swirl-type combustors

Williams et al. [43] report that NOx emissions were low for lean combustion in air and for combustion in CO_2-diluted oxygen for all stoichiometries. The trends in NOx emissions for different fuels and ϕ were found to correlate with the adiabatic flame temperatures and the calculated equilibrium O atom concentrations consistent with the importance of the Zeldovich and N_2O routes of NO production. CO emissions near the stoichiometric point, where dilute-oxygen power systems would necessarily operate, were insignificant until ϕ >0.95. At this point, emissions rose more rapidly for combustion in O_2–CO_2 mixtures than for combustion in air. Other than this minor difference, the presence of high concentrations of CO_2 in the CO_2-diluted oxygen flames was not found to have a significant impact on burner performance or emissions. Operation of the near-stoichiometric CO_2-diluted oxygen flames at oxygen levels of 20–24% was found to be promising for achieving very low emissions of both CO and NOx [43].

Lee et al. [44] find that in most of their tested cases, CO below 10 ppm is emitted, i.e. almost complete combustion, but in the case of steam dilution at 30 kW, CO emissions are increased exponentially according to the dilution ratio. This result means that the dilution system of an IGCC plant should be cautiously operated by monitoring the CO emission for the better fuel efficiency. The dilution of syngas with non-flammable gas decreases NOx emissions, and the amount of NOx reduction per unit power is logarithmically related to only the diluent's heat capacity which is the product of mass flow rate of the diluent and constant pressure heat capacity. This result can be used for controlling, adjusting, and predicting the NOx emission of an IGCC plant that uses fuel dilution technology for NOx reduction.

Two experimental papers report results for a swirl-type burner with partially premixed syngas combustion of syngas at atmospheric conditions which are similar to the CECOST burner. Ballachey et al. [45] investigates a swirling syngas flame. The ratio of CO to H_2 is 1, and a content of CO_2 of 15% and 25% is investigated. Flow imaging is realised by PIV and the LBO and FB limits are recorded. Another relevant syngas experiment with a swirling flame is reported by Samiran et al. [46], who investage a fuel mixture with $CO/H_2 \approx 1$, and a content of CO_2 between 5 and 25%, at 5% CH_4 content. The findings for LBO limits, luminosity imaging of flame shape, and emission data are reported.

A highly relevant simulation paper of LES of swirl-type premixed combustion

in a model combustor is presented by Li et al. [47]. The fuel is characterised by CO/H_2=1 and a content of CO_2 between 5-45%. The effect of syngas dilution with CO_2 is stated to be a decrease of the size of the IRZ, explained by a decrease of the effect of thermal expansion with increasing dilution. They conclude this from the observed more compact flame and smaller high temperature zone.

Chapter 3

Simulation of turbulent premixed swirl-stabilised flames

3.1 LES of turbulent premixed swirling flames

LES is an attractive approach for the study of gas turbine combustion dynamics, with a highly unsteady flow field dominated by turbulence motions that can be adequately resolved numerically. Models for subgrid scale (SGS) turbulence and for turbulent combustion are required for closure in LES. The small-scale turbulent motions are more isotropic and universal, and less affected by boundary conditions. Therefore simple models can represent their behaviour. The purpose of the SGS turbulence model is to mimic the transfer of energy associated with the energy cascade: to drain energy from the resolved large eddies to the smaller SGS eddies. Eddy-viscosity models based on Boussinesq's hypothesis, like the Smagorinsky model, are often used. However, Smagorinsky-type SGS models require wall functions to tune the anisotropic flow properties near boundaries. Another limitation is that the kinetic energy backscatter phenomenon is not considered. Dynamic models (Germano) which relax the equilibrium assumption of Smagorinsky-type models by calculating the model coefficients from the resolved scales during the simulation based on the scale-invariance assumption [41].

For turbulent reacting flows in the LES framework the detailed flame structure is often not resolved and combustion models are necessary at SGS. Without a SGS combustion model, the global burning rate is often underpredicted, since the unresolved flame is wrinkled at scales below the LES resolution. SGS combustion models used for the simulation of turbulent premixed swirling flames are reviewed by Huang & Yang [41] in 2009.

3.1.1 SGS models used in recent studies

SGS models used in recent studies of swirling premixed flames include transported probability density (PDF) approach, e.g., [48], flame surface density (FSD) SGS closure [49], flamelet generated manifolds (FGM) closure [50], level-set G-equation with presumed PDF SGS closure [51–53], etc.

Jones et al. [48] report good agreement with experiments on the TECFLAM premixed swirl burner for LES with the SGS PDF/stochastic field method. The Smagorinsky SGS viscosity is used for transport, and the linear mean square estimation closure (LMSE) is used for micro mixing.

Butz et al. [49] also investigate the TECFLAM swirl burner by means of LES. They apply the static Sigma model for the closure of the SGS stresses, using an algebraic scalar dissipation rate closure to model the filtered reaction rate. They report reasonably good agreement with experimental findings, very similar to results obtained based on flame surfcase density (FSD) closure approaches.

Zhang et al. [50] successfully use the dynamic Clark model for LES of the Sydney swirl burner for a comparison of the dynamic-thickened flame — flamelet-gernerated manifold (DTF-FGM) and presumed probability density — FGM (PPDF-FGM) SGS combustion models. The dynamic Clark model is a sum of the gradient model (nonlinear/tensor-diffusivity model) and the Smagorinsky eddy-viscosity model, using a Taylor expansion of the filtered velocity to determine the SGS model coefficients.

Nogenmyr et al. [51, 52] and Carlsson et al. [53] simulate swirling turbulent premixed methane/air flames stabilized in a low-swirl burner using LES with level-set G-equation coupled with detailed chemistry. Stretched laminar premixed flame profiles calculated in a counter-flow flame configuration with detailed chemical kinetic mechanisms were tabulated as a function of level-set G-function and flame stretch rate, which were integrated to the flow simulation using presumed PDF function. They show that the model can capture the flame structures, the effect of ambient dilution on the flames, and the shear layer stabilization mechanism of the flames.

The sensitivity of LES to SGS velocity modelling for premixed combustion, including swirling flames, is reviewed by Langella et al. [54].

3.1.2 Wall models for LES

The use of wall models in LES of complex flows is reviewed by Piomelli [55], and again, 10 years later, by Bose & Park [56]. The latter points out that the assumption about the alignment of the wall stress with the LES velocity at y^* may be invalid for swirling flows. The off-wall location y^* is the position where the LES is coupled to the wall model.

John-Puthenveettil & Jakirlić [57] assess the performance of adaptive wall functions for near-wall treatment in LES, including a case of isothermal flow in a swirl combustor. They conclude that the application of adaptive wall functions results in good agreement with PIV data for the investigated case with $15 < y^+ < 25$.

3.1.3 Criterion of LES mesh resolution and LES quality

A review on the influence of the mesh resolution on LES is provided by Boudier et al. [58]. Another review of mesh resolution in LES, especially for unstructured meshes, is given by Addad et al. [59].

The impact of mesh resolution on LES is demonstrated by the results reported by Benard et al. [60] who report LES results for the DLR PRECCINSTA premixed swirl burner for different levels of mesh refinement from 1.7 (NAD1; $\Delta = 1.2\,mm$) to 877 (NAD4; $\Delta = 0.15\,mm$ in the flame region) million cells. The simulations use non-adiabatic boundary conditions and a skeletal chemistry approach coupled with the dynamic thickened flame model. Excellent agreement with experimental data is reported only for the finest mesh.

Celik et al. [61] and Gant [62] five years later review various criteria to assess whether the grid resolution is adequate for LES. However, both conclude that a grid independence study is strongly recommended in every case.

3.2 Boundary conditions

A general review of LES, including a discussion on boundary conditions, is given by Yang [63]. Swirl generated by injectors is discussed and the generation of inflow boundary conditions is listed as one of the major challenges of LES. A detailed review of boundary conditions for LES can be found in Dhamankar et al. [64]. Another review of LES boundary conditions, namely inlet conditions, is given in Tabor & Baba-Ahmadi [65]. Different approaches to generate inlet conditions of fully developed swirling flow are outlined. In general, two categories of inlet conditions can be distinguished: synthesis inlets and precursor simulation methods. An example for the implementation of a synthesis LES inlet boundary condition is the divergence-free synthetic eddy method (DFSEM) available in OpenFOAM since version v1606+. With this boundary condition, turbulent eddies are continuously injected at the inlet patch to generate coherent flow structures to enhance the establishment of fully developed turbulent flow.

Burners with axial swirlers in the literature

Only certain gasturbine model combustors feature an axial swirler, where a number of blades generate the tangential momentum. These blades represent a modelling challenge for meshing and wall treatment, compared to radial-type swirl generators. Examples for axial-type swirlers are:

- The MIT swirl burner described by Taamallah et al. [19, 21, 66] for which LES results are reported.
- The EV/AEV half-cone swirl burner [67].
- The TARS burner [68].
- The swirling combustor investigated by Zheng et al. [69] who report LES results.

One way to avoid the challenge of modelling the swirler geometry and near-wall flow, is to use a swirl inlet profile boundary condition. A successful application of such an inlet condition is presented by Foroutan & Yavuzkurt [70] for the simulation types DES (Detatched Eddy Simulation), URANS SST (unsteady RANS with Menter's Shear Stress Transport turbulence model) and PANS (Partially Averaged Navier-Stokes).

3.2.1 Boundary conditions for compressible flow simulation

Noh et al. [71] reproduce experimental observations of instabilities in a swirl-stabilised premixed combustor applying LES and numerical dynamic mode decomposition. A compressible flow solver is used on a structured grid. The dynamic Smagorinsky model is used for SGS modelling. The sub-grid probability density function approach is chosen for the unresolved interaction between turbulence and chemistry. A reduced mechanism is used together with the Eulerian stochastic field method. At the outlet boundary, pressure reflection at open boundaries is modelled by applying a Navier-Stokes characteristic boundary condition (NSCBC). The non-linear behaviour of the thermo-acoustically excited flame is captured in agreement with experiments.

Hermeth et al. [72] evaluate the effect of equivalence ratio fluctuations on flame dynamics of a premixed swirling flame. LES of compressible flow is performed with the classic Smagorinsky SGS model. SGS wrinkling and turbulence/chemistry interaction is modelled using an efficiency function. Non-reflecting NSCBC are specified at the inlet and outlet. Wall-functions are applied. Mechanisms affecting the dynamic flame response are revealed by comparing a technically and a fully premixed case. The dynamic response of the mixing process is identified.

3.3 Literature study: isothermal flow through swirl-type gas turbine model combustors

There are several gasturbine model combustors to study non-premixed and premixed swirl-stabilised flames. A selection is presented in the following to give an overview over which mesh types, simulation approaches, and inlet conditions have been reported as successful in the literature.

3.3.1 DLR dual swirl burner

One of the best documented swirl-type gasturbine model combustors is the DLR dual swirl burner [73]. The following is an overview over the meshing stategies, and simulation model performance reported in the literature.

- Widenhorn et al. [74] present results for cold flow using the software CFX with a mesh of 1.6 million unstructured hexahedral cells. They compare the performance of the simulation approaches URANS SST, SAS (Scale-Adaptive Simulation), DES and validate the predictions with PIV data.
- In a later study, Widenhorn et al. [75] report flow fields for cold flow using the software CFX for meshes of 1.9, 2.6 million unstructured tetrahedral and hexahedral cells. The modelling approaches URANS SST, SAS, DES are validated with LDA data.
- Benim et al. [76] present results for cold flow using the CFD solver OpenFOAM with meshes in the range of 2-16 million hexahedral cells, including the farfield at outlet. The simulation types URANS SST, URANS RSM (URANS with Reynolds Stress Model for turbulence), and LES are compared to LDA data.
- Chen et al. [77] present results for cold flow (OpenFOAM) for meshes with 12-20 million tetrahedral cells, including the far-field and fuel inlet slots of the burner. LES results are validated with LDA data.
- In later study, Chen et al. [42] present results for cold flow (OpenFOAM) for a mesh of 15+3 million tetrahedral cells, including the far-field and fuel inlet slots as well as a refined nozzle (+3 million cells). LES flow field is validated with LDA data.

3.3.2 PRECCINSTA premixed swirl burner

Another well-studied gasturbine model combustor with a swirl-stabilised flame is the PRECCINSTA burner [67], where fuel and air enter the burner in a premixed

state. Isothermal flow simulations of this burner configuration reported in the literature are presented in the following.

- Lartigue et al. [78] present results for cold flow using the CFD solver AVBP for a mesh of 3 million tetrahedral cells. LES validation with LDA data is demonstrated.
- Roux et al. [79] present results for isothermal flow (AVBP) with the same computational grid of 3 million tetrahedral cells including the far-field. They demonstrate validation of LES flow fields with LDA data. The WALE (Wall-Adapting Local Eddy-viscosity) SGS model is used for this study.

3.3.3 CERFACS dual swirl burner

Yet another swirl-type gasturbine model combustor is the CERFACS dual swirl burner. It is investigated by numerical simulation by Davillier et al. [80], who present results for isothermal flow (AVBP) for meshes with 1–11 million tetrahedral or hexahedral cells. Detailed mesh effects on the swirl are studied. Their findings from LES simulations are validated with PIV data.

3.3.4 CECOST swirl burner

The premixed swirl-type gasturbine model combustor with axial swirler investigated as part of this thesis is another example. The CECOST burner features four blades, and has been studied both numerically with LES and experimentally with laser-based imaging techniques [81]. This setup is described in detail in chapter 4.

Chapter 4

CECOST burner, experimental setup and methods

In this section, the experimental setup of the CECOST swirl-type model combustor is described. The burner was designed by Hodzic [81], and was 3D printed. The burner was installed at the Combustion Physics lab of Lund University where systematic experiments have been carried out using laser based diagnostic methods, including chemiluminescence imaging, planar laser induced fluorescence (PLIF) of OH and CH_2O, particle image velocimetry (PIV).

4.1 Experimental setup

Figure 4.1 shows a schematic representation of the burner. Note that the burner is mounted vertically below an exhaust vent. Dry air is supplied by a blower (Rietschle SAP 300) with a maximum air flow rate of 55 g/s at room temperature. The blower rotational frequency is adjusted in the control routine to set a certain mass flow rate of air. A thermal mass flow meter measures the air flow (Eldridge MPNH-8000) with an accuracy of ±1% reading and ±0.5% full load). A pipe elbow connects the blower with the vertically mounted modular CECOST burner. The flow expands into a plenum with a series of metal sheet grids of different grid size. The grids with square cells straighten the flow [82] and reduce the level of turbulence [83]. These grids are located just upstream of the burner section shown in Fig. 4.1.

The fuel mass flow is controlled by mass flow controllers (Alicat Scientific MC-100SLPM) with an accuracy of ±0.8% reading and ±0.2% full load). The air enters a plenum that is connected to the blower by a pipe with an elbow

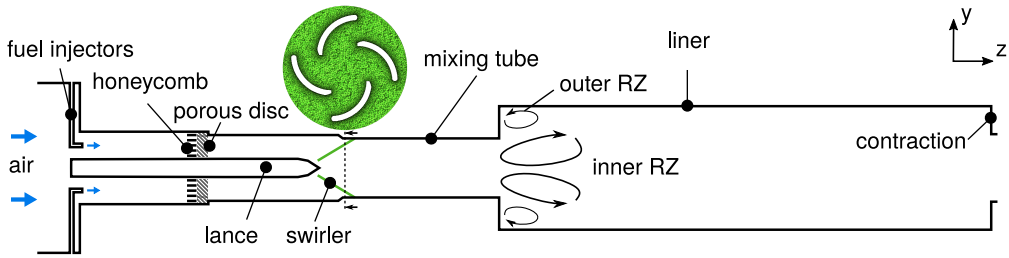

Figure 4.1: Schematic representation of the CECOST burner setup showing the modular components. The swirler blades are indicated in green, and a cross-section of the computational mesh is provided to help visualise a cut-plane normal to the flow direction.

which directs the flow to the vertical direction. At the downstream end of the plenum, where the circular cross section is reduced to 56 mm by a forward facing step, four single-point injectors are mounted. Two of these injectors are for the injection of fuel, and two for the injection of air seeded with particles when PIV measurements are performed. The fuel/seeded air jets and the bulk air flow enter the first section of the annular channel between the steel rod, on which the swirler blades are mounted, and the outer wall. This first section represents approximately one third of the total length of the mixing tube, the section between the injectors and the expansion into the rectangular combustion chamber. At the end of this section, two discs are mounted: one is a type of honeycomb and the other consists of a porous material. These two discs stop the potential upstream propagation of the flame in the fuel/air mixture by wall quenching. The slot width in the honeycomb material is approximately 0.5 mm, and therefore even below the quenching distance of stoichiometric H_2-air mixture, which ensures a reliable function as flame-arrestor for all investigated fuels.

The next section of the mixing tube is in an annular channel of outer diameter 54 mm and an inner diameter of the rod of 16 mm. At the end of the rod, four swirler blades are mounted. The four blades of this axial swirler are of the shape of a quarter-cone surface and have a thickness of 2 mm. Downstream of the swirler, in the last third of the mixing tube, the cross section decreases further to a diameter of 48 mm. As can be seen in Fig. 4.2, this last section of the mixing tube is constrained by three main parts: the 3D-printed swirler corresponds to a short section of the wall, then a transparent quartz tube of a length of 100 mm allows optical access to large parts of this last mixing section, finally, a 20 mm thick metal plate constitutes the final section of the mixing tube, and also holds the quartz combustion chamber liner on its upper surface. Here, the swirling flow expands from the 48 mm diameter tube to a 100x100 mm^2 combustion chamber with a square cross section. This chamber has a length of 400 mm and features a nozzle of 55 mm diameter as outlet.

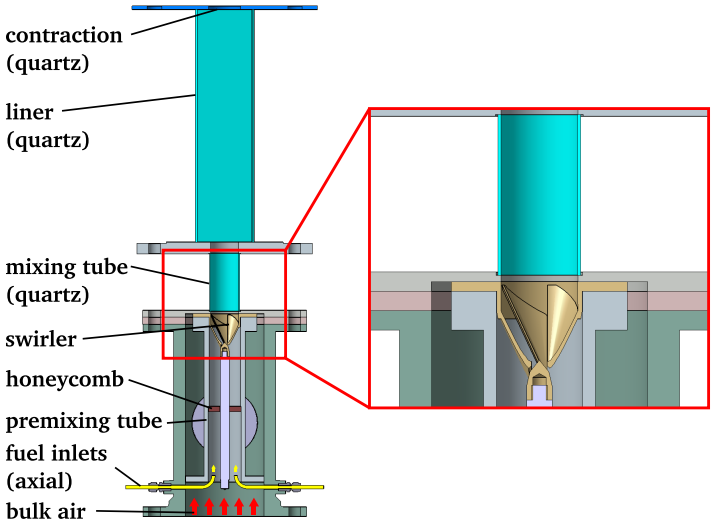

Figure 4.2: Cut plane of the CAD model of the CECOST swirl burner with labeled components and showing a detail of the swirler blades and quartz mixing tube section.

For each fuel blend, the fuel and air mass flow rates are computed based on two input values: the desired Reynolds number (Re) and fuel-air equivalence ratio (ϕ). In the following, the procedure to calculate the mass flow rates for mixtures of CH_4 and NH_3 from 0 to 100% is demonstrated. Table 4.1 shows the density ρ and dynamic viscosity ν of the two fuel components and air at atmospheric conditions and a temperature of 300 K. For the calculation of the mass flow rates, it is assumed that the dynamic viscosity of any air-fuel mixture equals that of air, which is a reasonable assumption considering the values shown in the table.

Table 4.1: Overview over density and kinematic viscosity of selected gases at atmospheric pressure and 300 K [84]

	NH_3	CH_4	air
$\rho\,[\mathrm{kg/m^3}]$	0.6898	0.644	0.01762
$\nu\,[\mathrm{m^2/s}]$	$14.7{\cdot}10^{-6}$	$17.27{\cdot}10^{-6}$	$15.67{\cdot}10^{-6}$

Denoting the mole fraction of NH_3 in the fuel, x_{NH_3}, by a and that of CH_4 in the fuel by b, the mass flow rate of air $\dot{m_{air}}$ in [kg/s] is calculated to be

$$\dot{m}_{air} = \rho_{air} * \dot{V}_{air} = \rho_{air} \frac{ReD\nu\pi}{4} \frac{1}{1 + \frac{4\phi}{4.67(3a+8b)}} \tag{4.1}$$

and the volumetric flow rate of fuel $\dot{V}_{fuel}$ in [l/min] is calculated to be

$$\dot{V}_{fuel} = \dot{V}_{air}\phi\frac{4}{3a+8b}\cdot 60\cdot 10^3 \tag{4.2}$$

and the respective volumetric flow rates of NH_3 is

$$\dot{V}_{NH3} = a\cdot\dot{V}_{fuel} \tag{4.3}$$

and the mass flow rate of CH_4 is

$$\dot{m}_{CH4} = \rho_{CH4}\cdot b\cdot\dot{V}_{fuel} \tag{4.4}$$

based on the stoichiometric relation

$$(a\,\mathrm{NH_3} + b\,\mathrm{CH_4}) + (\tfrac{3\,\mathrm{a}+8\,\mathrm{b}}{4})(\mathrm{O_2} + 3.76\,\mathrm{N_2}) \longrightarrow b\,\mathrm{CO_2} + \tfrac{3\,\mathrm{a}+4\,\mathrm{b}}{2}\,\mathrm{H_2O} + (\tfrac{\mathrm{a}}{2} + 3.76\cdot\tfrac{3\,\mathrm{a}+8\,\mathrm{b}}{4})\,\mathrm{N_2}$$

4.2 Measurement techniques

The measurement techniques used for the investigation of the CECOST swirl burner are high-speed chemilumninescence imaging of OH (OH-CL), planar laser-induced fluorescence (PLIF) of OH and particle image velocimetry (PIV). The diagnostic setup and processing techniques are described in detail in Refs. [81, 85], as well as in Papers I and II. In the following, a brief overview over the applied diagnostic techniques is given.

The OH-CL imaging, a line-of-sight technique with inherent limitation, covers the whole optically accessible section of the CECOST swirl burner, from the quartz mixing tube to the outlet nozzle of the combustion chamber. The strength of this technique is that it allows the study of stable flames, as well as of unstable flames during (intermittent) flashback events or near blow-off. The high frame rate of up to 15,000 fps allows the analysis of transient phenomena, and advanced postprocessing methods like for example proper orthogonal decomposition (POD). The complementary strength of the OH-PLIF technique is to give a picture of the flame on a small scale. This technique shows the flame structure at a vertical centreplane of the combustor, from the chamber inlet up to a height of approximately 60 mm. The temporal resolution is lower, at 10 Hz. These two techniques are thus complementary and allow to image the global flame shape at high frequency, and a chosen section in high spatial resolution.

PIV is performed for selected operating conditions, both for isothermal flow and for reacting flow. The imaging section and frequency corresponds approximately to the parameters of the OH-PLIF technique, with high spatial resolution, albeit for a small section of the combustion chamber, and at relatively low temporal resolution.

4.3 Simulation setup

4.3.1 Simulation in OpenFOAM

The open source CFD package OpenFOAM [86] is used to carry out the simulations. The flow is approximated as low Mach number flow. The PIMPLE algorithm couples pressure and velocity. Every time step consists of one PISO and two PIMPLE loops. The transport equations are discretised according to the finite volume method. Second-order schemes are used to discretise the Laplacian, convection, and gradient terms. The implicit second-order time scheme 'backward' is used for integration in time. An implementation of the Smagorinsky sub-grid scale (SGS) turbulence model with C_s=0.13 is used to close the residual stress tensor. The time step size is selected in each case to fulfil CFL≈0.90. A top-hat velocity profile is set at the inlet, and a constant gauge pressure of 0 Pa is applied at the outlet. At the walls, a no-slip condition is applied. The remaining boundary conditions are of von Neumann type, i.e. with zero gradient. All presented flow fields are averaged over several flow-through times.

For parameter studies, different wall functions were applied, the default wall function for ν_t being the *nutKWallFunction*, and most promising the *nutUSpaldingWallFunction*. In another parameter study, the WALE model was used instead of the Smagorinsky SGS model. A description of these wall functions can be found in the code documentation [86].

4.3.2 Meshing

Unstructured tetrahedral meshes from 800,000 to 50 million cells are used to discretise the computational domain including the CECOST burner swirler, the mixing tube and the combustion chamber sections. The overall maximum y^+ value is 100 and a typical minimum value is 0.01. The meshes were generated for either the full domain, including the injectors, or for selected parts of the burner, the minimum extent domain covering only the swirler blades and the mixing tube. The meshing tool ANSYS ICEM is used to create unstructured meshes in an octree stage followed by a delauney flood fill. The findings of a mesh-sensitivity study are presented in section 5.1.4.

A cut-plane view through a mesh of intermediate resolution, with refinement at the blade wall, is shown in Fig. 4.3. It can be observed that a majority of the cells in the vicinity of the blades. The blade shape with rounded trailing edge and thinner leading edge is based on the 3D-printed swirler. This cut-plane allows to understand the design process of the swirler, where a 2 mm thick sheet following a cone surface is cut in four, and then each piece is moved by an offset of 5 mm in radial and tangential direction.

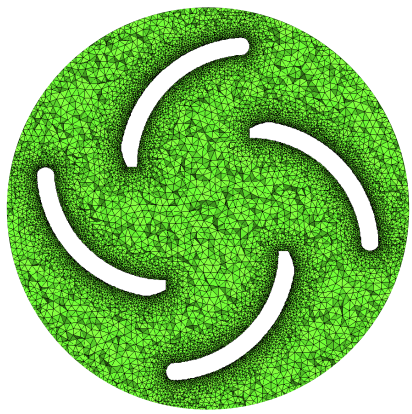

Figure 4.3: Cut-plane view of the swirler region of a mesh of intermediate resolution. The blade shape with rounded trailing edge and thinner leading edge is modelled based on the 3D-printed swirler.

Chapter 5

Results and Discussion

This chapter presents selected results from experimental and numerical investigations of different aspects of the CECOST swirl burner, with focus on topics not reported in Papers I and II.

5.1 Structure of turbulent swirling flows

The flow structure in the CECOST swirl burner was measured by PIV in a section of the combustion chamber, just downstream the expansion into the chamber. Figure 5.1 shows isothermal flow fields calculated for air flow at a Reynolds number of 20,000. LES was performed for a computational domain indicated in Fig. 5.1(a), where a red dashed rectangle indicates the region for which the averaged LES flow field is shown in Fig. 5.1(b). This section corresponds approximately to the section for which PIV data is available. U_y denotes the flow component normal to image, the tangential velocity is U_θ. Figure 5.1(d) shows a representation of normalised vectors for the in-plane velocity components in this cutplane. Positive bulk axial velocity can be seen at the expansion, splitting into two diverging jets impinging on the combustor wall towards the downstream end of the shown section. At the top and on the left and right bottom corners, negative axial flow regions are observed. The central one is in the following referred to as inner recirculation zone (IRZ), and the outer recirculation zone, observed all around the step, is referred to as outer recirculation zone (ORZ). The IRZ formation is due to the phenomenon of vortex breakdown, where a swirling jet that expands develops a recirculation zone at its centre, if the ratio of the strength of the swirling motion relative to the axial momentum of the jet is above a certain threshold value. This criterion will be described in more detail when the non-dimensional swirl number (Sw) is introduced in section 5.1.1.

The averaged in-plane velocity in vector form, without normalisation, can

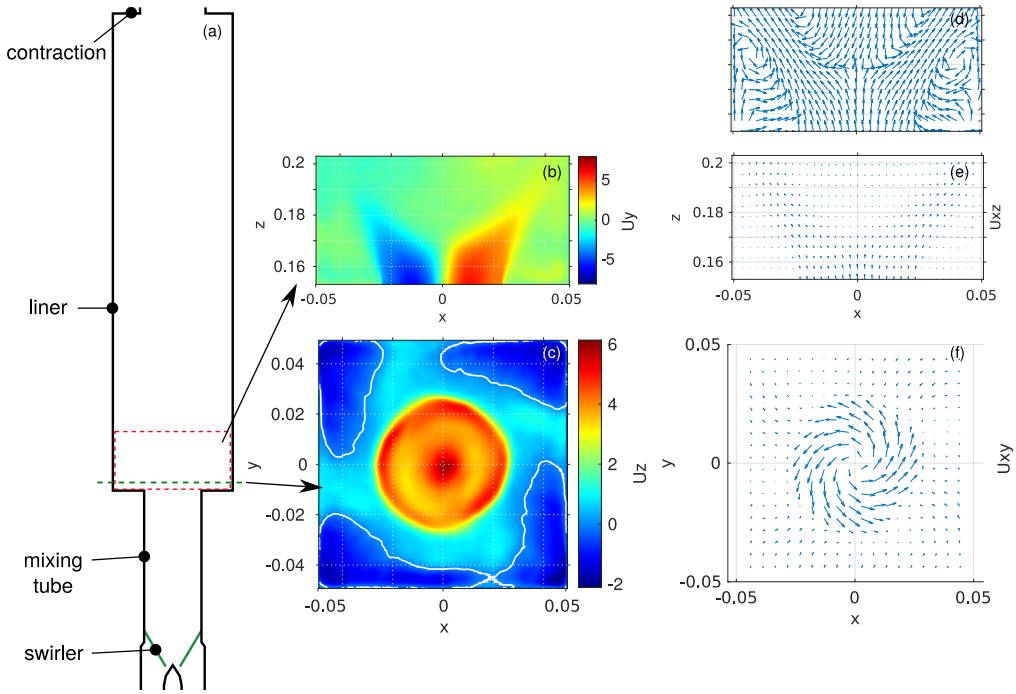

Figure 5.1: Averaged LES of isothermal flow at Re=20,000: axial (U_z), tangential (U_y), and in-plane velocity components at selected cut-planes.

be seen in Fig. 5.1(e). It can be observed that the in-plane velocity magnitude is highest in slice of the turbulent swirling jet, and lower in the recirculation regions. Marked by a blue dashed line in Fig. 5.1(a), the axial position of a horizontal cut (in flow normal direction) is indicated. The cut plane is 5 mm above the dump plane, and the corresponding flow field is shown in Fig. 5.1(c), which shows the axial flow speed distribution, and (f), which shows the in-plane velocity component in vector form. It can be observed that the flow field in this cutplane is not axi-symmetric, the ORZ varies in strength tangentially. But the swirling motion of the incoming flow can clearly be observed. The choice of a combustion chamber with square cross section is due to previous observation of reflections which reduced the quality of laser diagnostics data when using a circular chamber.

The structure of the isothermal flow predicted by LES at Re=20,000 and 10,000 is compared to PIV data in Fig. 5.2. The location of the horizontal lines in the centre cut plane of the combustion chamber along which the data is compared, are indicated as red dashed lines in Fig. 5.2(c). Further, it can be observed that no PIV data is available near the walls of the combustor, where the signal quality is significantly reduced by reflections. For the locations where

PIV data points are available, these are indicated with squares and compared to the averaged LES results, shown as profiles with solid lines. The height above the dump plane of the combustor, z, is indicated. The lines at a height of 10, 20, 30, 45, and 60 mm are selected because they represent the overall flow structure well. The bottom row of figures is closed to the dump plate. Figure 5.2(a) shows the average axial velocity component for Re=10,000, while column (b) shows the same for Re=20,000. The axis scale of the higher Re case is exactly double that of the low Re case, so that in case of Reynolds number independence, the profiles in (a) and (b) would be of same shape at same height. This is indeed almost the case, for PIV as well as simulation results. Note that the experimental data set shows a pronounced asymmetry. In the radial plots, this shows as two distinct profiles of PIV data, one for the left and one for the right side of the combustor.

It can be observed that the profiles of PIV data and simulation results for the radial profiles of averaged axial flow component follow somewhat similar trends, especially if the lowest and highest profiles are excluded. At these positions, the signal quality might be influenced by a weaker laser sheet at the extremities, or reflections at the dump plate. The same observation is made for the radial profiles of RMS of the axial velocity component, which is shown for lower and higher Re in Fig. 5.2(c) and (d). Note the different scale for RMS from LES and PIV. These separate scales are necessary to compensate for the fact that the cell size in the simulation is much smaller than the spatial resolution of PIV, and the low temporal resolution of PIV, compared to LES, where statistics are collected at a rate several orders of magnitude higher than for the PIV technique.

The asymmetry of the experimental data set and the assumptions in the LES setup do not allow a conclusion whether the agreement between experimental data and simulation results is acceptable. Before moving on to reacting flow simulations, several parameter studies for the numeric setup are performed. One non-dimensional number to compare the effect of different parameter changes is the swirl number (Sw). This parameter is introduced in the next section.

5.1.1 Flow structures in the mixing pipe

The reduced swirl number [87] is one of the parameters used to describe the character of a swirling flow. If the average radial profiles of the axial velocity component $\overline{U}_{ax}$ and of the tangential velocity component $\overline{U}_{\theta}$ are known, S can be determined as

$$S = \frac{\int_0^R \overline{U}_{ax}(r)\,\overline{U}_{\theta}(r)\,r^2\,dr}{R\int_0^R \overline{U}_{ax}^2(r)\,r\,dr}, \tag{5.1}$$

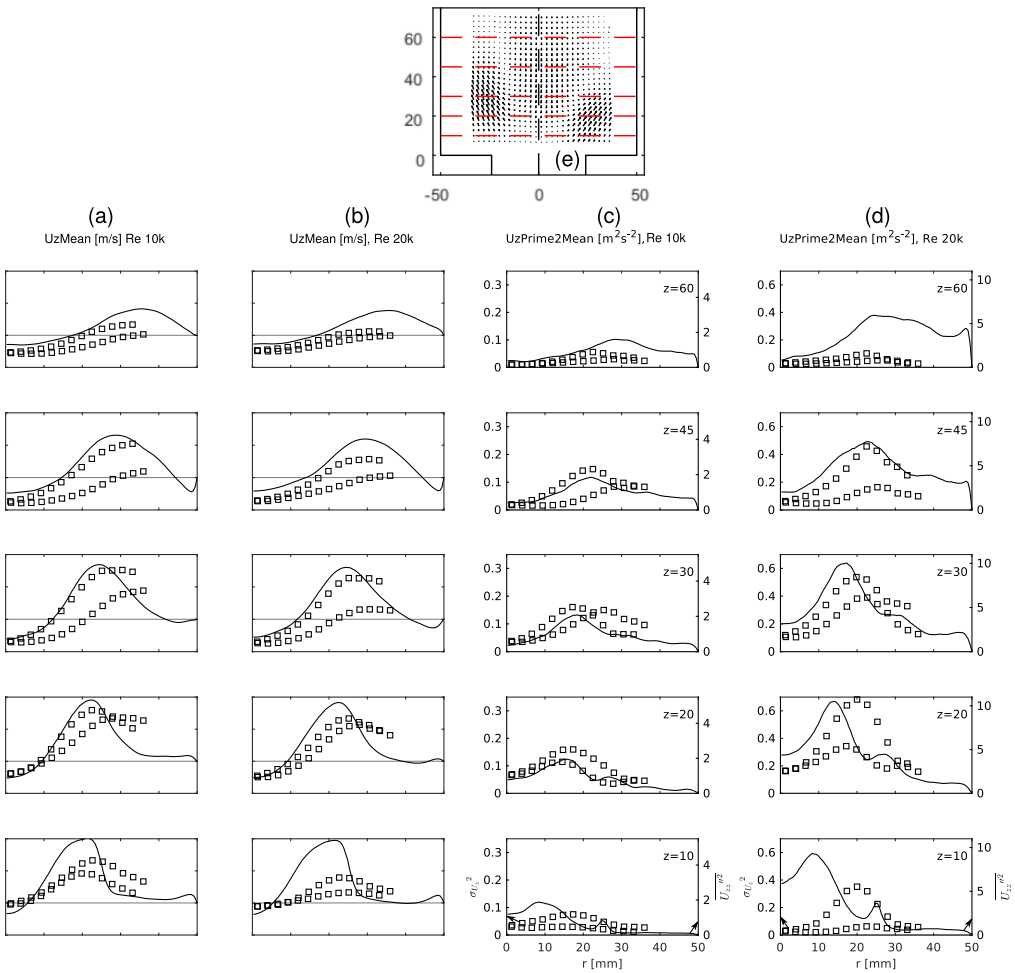

Figure 5.2: Comparison of isothermal flow averaged LES results with PIV data for Re=10,000 and 20,000. The mean and RMS of the axial velocity component is shown. Note the different scale for RMS from LES and PIV.

where r is the radius and R is the tube radius. More generally, the reduced swirl number is calculated as

$$S = \frac{\sum_{0}^{R} \overline{U}_{ax}(r)\,\overline{U}_{\theta}(r)\,r^2\,dA}{R\sum_{0}^{R} \overline{U}_{ax}^2(r)\,r\,dr}, \tag{5.2}$$

where dA is an infinitesimal part of area in a flow-normal cut-plane. The thus defined non-dimensional number allows a comparison of different swirling flows,

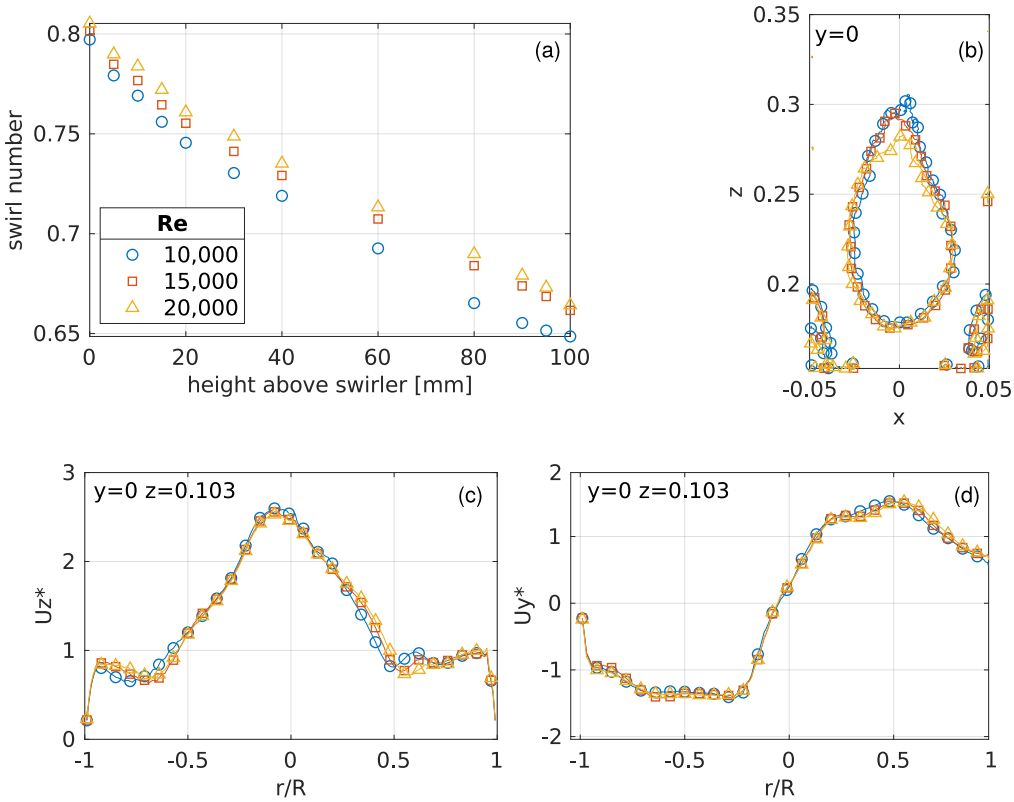

Figure 5.3: Comparison of swirl number profile along the mixing tube (a), contours of IRZ and ORZ (b), as well as profile of average axial (c) and tangential (d) velocity component in the mixing tube are compared for three different values of Re.

independent of the Reynolds number or tube diameter. In the following section, the effect of Reynolds number on the flow structure is investigated, as this would allow the restriction of future investigations to a single value of Re.

5.1.2 Reynolds number independence

Figure 5.3(a) shows the swirl number profile along the mixing tube for three different Reynolds numbers, 10,000, 15,000 and 20,000, from directly above the swirler, to close to the expansion into the combustion chamber. It can be observed that the value of the swirl number decreases further downstream in the mixing tube. Furthermore, it can be observed that the profiles of Re=15,000 and 20,000 match quite well, while the case corresponding to the lowest value of Re results in a slightly lower swirl number, especially at the downstream end of the mixing tube. However, for Reynolds numbers above 15,000, the swirl properties are observed to nearly Reynolds number independent.

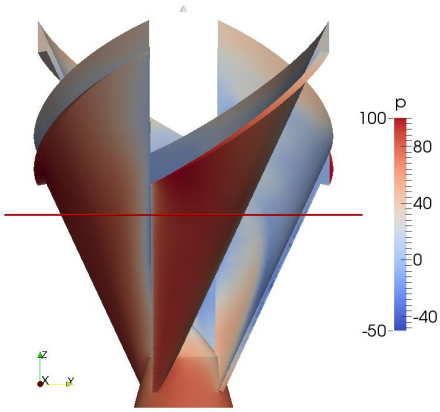

(a) Pressure distribution on swirler surface with cross-section location indicated by the red line.

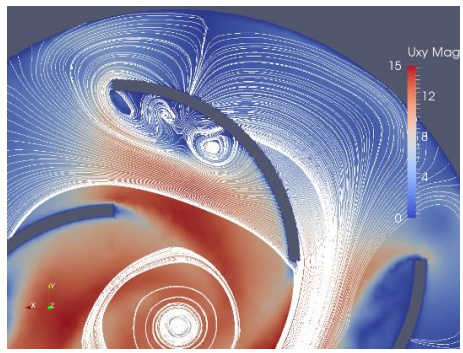

(b) Velocity amplitude in a flow-normal cross-section through the swirler, with streamlines visualising a separation zone.

Figure 5.4: Visualisation of separation zones from averaged LES of isothermal Re=20,000 case with 30 million tetrahedral cell mesh.

This conclusion is further solidified by observing the position and shape of the IRZ and the ORZ in Fig. 5.3(b), which shows that the recirculation zones match well for all three investigated Re cases, with only minor variations at the downstream tip of the IRZ. A very similar observation is made for Fig. 5.3(c) and (d), where the average profiles of the axial (c) and tangential (d) velocity components almost coincide for all three Re number cases.

In the next section, the flow field near the swirler blades is studied in detail.

5.1.3 Flow structures around the swirler

In this section, the flow near the swirler blades is described. Flow separation is observed in the wake of the leading edge of each blade. This separation zone is shown for a flow-normal cut-plane through the domain at a middle height of the swirler. The position of this cutplane is marked by a red line in Fig. 5.4(a). This figure shows the averaged pressure distribution on the surface of the swirler section from LES of an isothermal flow case at Re=20,000. The recirculation zone size can be estimated by the area of the low pressure region on the inside of the rightmost blade in (a). Figure 5.4(b) shows the average velocity magnitude in this flow-normal cross-section, with streamlines to visualise the flow pattern, especially the separation zone. This recirculation zone in the wake of the leading edge of each blade might be sensitive to small geometric variations, and will be the focus of future design studies.

In the following section, the findings of a mesh sensitivity study are presented.

5.1.4 Mesh-sensitivity study

In a first step, a mesh sensitivity study was performed for the domain between the honeycomb and the outlet of the combustion chamber. This domain includes a wide range of length scales to resolve, and even for meshes with up to 30 million cells, no convergence of the flow field between meshes of different resolution was observed. Therefore, the domain for the sensitivity study is limited to the section including the swirler and the mixing tube. A nozzle forms the outlet of this reduced domain, where the flow expands into the combustion chamber in the full domain. The nozzle is selected to avoid backflow. It was found that the nozzle does not change the flow field close to the swirler (data not shown here). This reduced-domain sensitivity study is presented in the following.

The reduced domain shape with outlet nozzle can be seen in Fig. 5.5(a). The averaged results of LES for isothermal flow at Re=20,000 are shown. From top to bottom the distribution of the magnitude of the axial component of the flow velocity is shown for four increasing levels of mesh resolution. The isocontour of zero axial velocity indicates the extent of recirculation zones. It can be observed that with increasing resolution, the central high axial flow speed region in the first half of the mixing tube becomes narrow, with higher peak value. For a detailed comparison of the four cases, Fig. 5.5(b) shows the radial profiles of the average axial (U_{ax}) and tangential (U_{θ}) component of the flow speed, normalised by the axial bulk flow speed, U_{in}. The two axial positions in the mixing tube, for which the profiles are compared, are indicated by dashed red lines in (a).

For both axial positions, '-100 mm', just downstream of the swirler, and '-120 mm', 20 mm further downstream, the profiles of axial and tangential velocity follow the same trend of a higher peak velocity for the case with highest mesh resolution, and the peak value of the other three cases in decreasing order of resolution. A further observation is that the difference in peak value between the two meshes of highest resolution is largest, indicating that the resolution is not converged. A future mesh sensitivity study needs to demonstrate what radial profiles the solution converges to for even higher resolution. It has shown that increasing the surface resolution alone does not yield a large difference in the profiles, as tested for a version of the finest mesh, but with the volume resolution of the second-finest mesh (not shown for brevity).

In the next section, the pressure drop over several of the components of the CECOST swirl burner is presented.

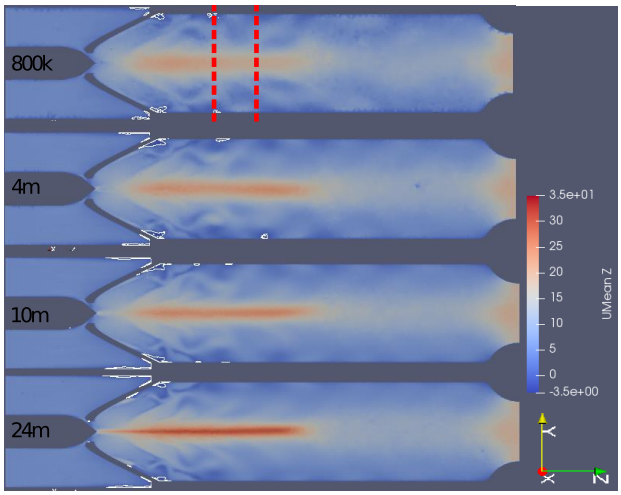

(a) Magnitude of axial velocity component with isocontour of zero for four different levels of mesh resolution.

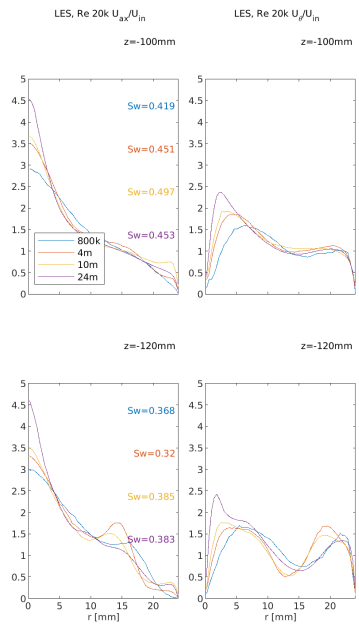

(b) Radial profiles of axial and tangential velocity component 100 and 120 mm upstream of the combustion chamber.

Figure 5.5: Mesh sensitivity study for reduced domain with nozzle. Averaged LES of isothermal flow at Re=20,000.

5.1.5 Pressure drop measurement and swirler measurement

The pressure drop was measured by a micromanometer with a measurement range up to 1000 Pa. A picture of the experimental setup to determine the pressure drop is shown in Fig. 5.6(b). The first tube (reference pressure p_1) is open to the ambient pressure, the second tube (measurement pressure p_2) is connected to the cavity upstream of swirler and mixing tube (see section 4). The pressure difference, Δp is determined as $\Delta p = p_2 - p_1$.

The air mass flow is increased in small steps until the pressure drop over the current setup reaches the limit of the range at 1000 Pa. This first step of measurements, repeated for different configurations is shown in Fig. 5.6(a). The pressure drop coefficient is then calculated based on the bulk flow speed in the mixing tube and the pressure drop as

$$\xi = \frac{2\Delta p}{\rho U^2}, \tag{5.3}$$

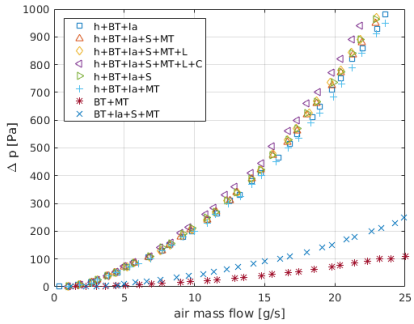

(a) Measurement of the pressure drop over mass flow rate of air.

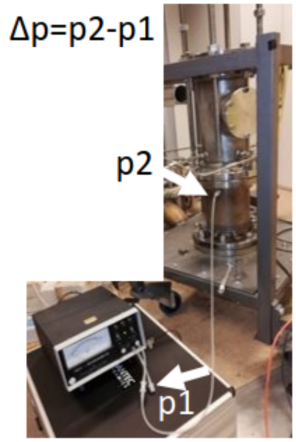

(b) The experimental setup.

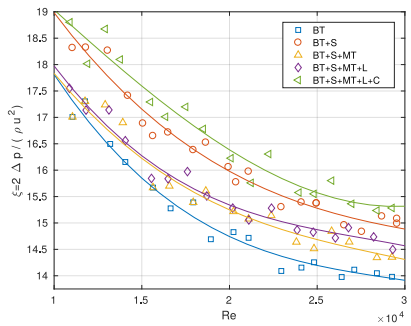

(c) The pressure drop coefficient for different setups.

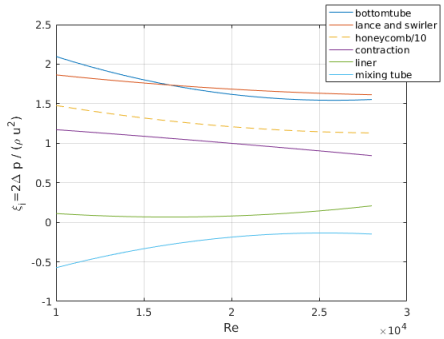

(d) The pressure drop coefficient per component.

Figure 5.6: Pressure drop measurement for isothermal flow.

where U is the bulk flow velocity in the mixing tube calculated from the air mass flow, ρ the air density at 300 K, and Δp the signal from the micromanometer.

Apart from determining the pressure drop coefficient of the swirler, the 3D-printed swirler's dimensions are measured and compared to the geometry in the computational model. Pictures of the swirler component are shown in Fig. 5.7(a) and (b), where the slot width, the distance between two blades, is indicated. This slot width is measured twice at each position for each of the four gaps using a caliper. The average of two profiles of the slot width for each gap is shown in Fig. 5.7(d), and the raw data in Fig. 5.7(c). The slot width is in agreement with the value in the CAD model, 7.82 mm. The difference between

(a) Picture of the swirler.

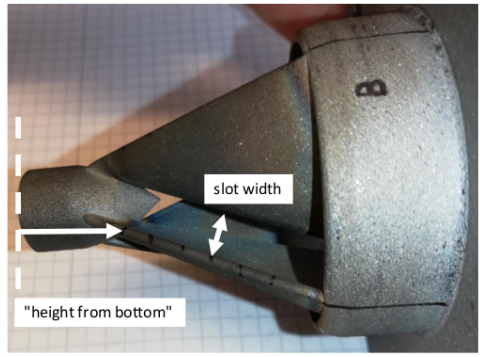

(b) Indication of slot width and height 0.

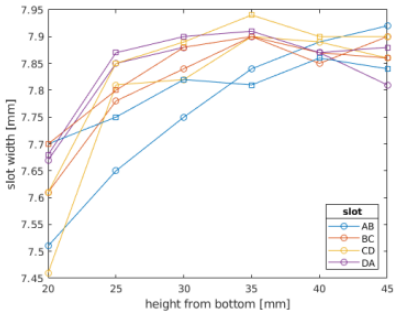

(c) Slot width over axial position for each gap.

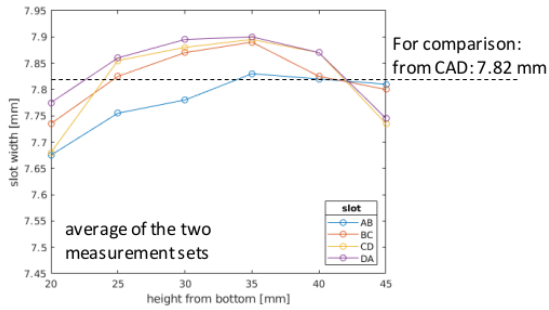

(d) Average slot width over axial position for each gap and comparison to CAD model.

Figure 5.7: Dimensions of the 3D-printed swirler and comparison to model geometry.

the slot width profiles of the four gaps is within measurement uncertainty.

A more accurate automated measurement, including the blades themselves, would allow to determine if the 3D-printed blades indeed correspond to the swirler geometry on which the simulations are based.

In the next section, the calculation of the laminar burning velocity s_L and the adiabatic flame temperature T_{ad} is presented. This data is used for the presentation of the experimental results for the stability limits for different fuels. Based on the fuel composition and the equivalence ratio, the corresponding values of s_L and T_{ad} are calculated.

5.1.6 Calculation of laminar burning velocity

The laminar burning velocity within the flammability limits for all investigated fuel mixtures was determined from premixed laminar 1D flames calculated in

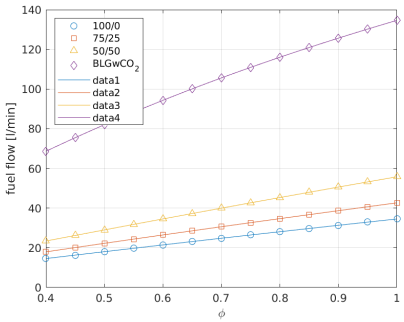

(a) Fuel flow rates for Re=10,000.

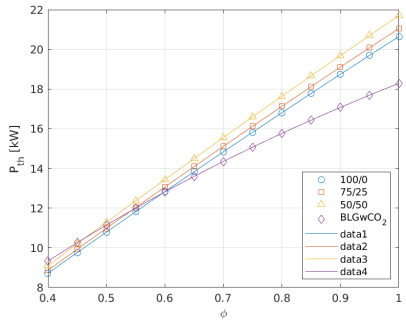

(b) Thermal power for Re=10,000.

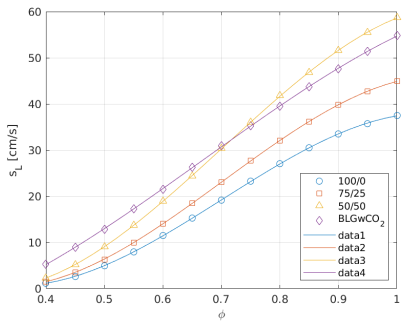

(c) Laminar burning velocity for different fuels.

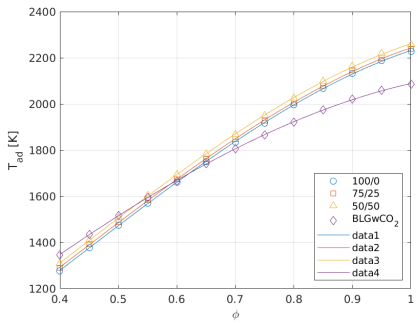

(d) Adiabativ flame temperature for different fuels.

Figure 5.8: 1D calculation of the laminar burning velocity and adiabatic flame temeprature of H_2-enriched CH_4 and syngas.

Cantera [88] using GRI-Mech 3.0 [89]. Figure 5.8(a) shows the fuel flow rates as a function of the equivalence ratio for different fuel blends at Re=10,000. The corresponding thermal power P_{th} is shown in Fig. 5.8(b). The values of s_L and T_{adi} are independent of the Reynolds number, and are given in Figs. 5.8(c) and (d) respectively.

It can be observed that the adiabatic flame temperature is similar for all CH_4/H_2 blends, while the values for syngas are lower at richer conditions, but higher at leaner conditions. For an equivalence ratio above approximately 0.7, the investigated syngas mixture has a slightly lower laminar burning

5.2 Flame structures

V, M, and Π shaped flames were observed, depending on Re, ϕ, burner configuration and fuel blend. The Π shaped flame was observed for H_2/CH_4 fuel blends for a certain burner configuration, but only for high values of ϕ. These findings are described in detail in Paper II, while Paper I describes the flame shape and operating range found for CH_4/air flames in a slightly different burner configuration.

Chapter 6

Summary of publications

Paper i: Flame investigations of a laboratory-scale CECOST swirl burner at atmospheric pressure conditions

A. A. Subash*, S. Yu, X. Liu, **M. Bertsch**, R.-Z. Szasz, Z. Li, X.-S. Bai, M. Aldén, D. Lörstad
Fuel, Volume 279, 2020, doi.org/10.1016/j.fuel.2020.118421

This paper discusses the operating range of the CECOST swirl-type gasturbine model combustor at atmospheric pressure. The burner is operated with either natural gas or industrially pure CH_4. The operating range is determined for a range of flow speeds (flow Reynolds number) as the stable region between flashback and lean blow-off. The flame dynamics are analysed by means of high-speed chemiluminescene imaging and PLIF imaging of OH and CH_2O. Flashback events are analysed by postprocessing of high-speed imaging data, among others modal analysis. CFD results for isothermal flow in the burner at different Reynolds numbers are discussed to support the conclusions from experimental observation.

The candidate contributed to the CFD part as well as the experimental campaign. For the CFD part, a geometry and grid dependence study was performed. Furthermore, the candidate provided the CAD figure and contributed to the operating range diagram. Apart from this, he was also involved in the revision process.

Paper ii: Investigation of turbulent premixed methane/air and hydrogen-enriched methane/air flames in a laboratory-scale gas turbine model combustor

X. Liu, **M. Bertsch**, A. A. Subash*, S. Yu, R.-Z. Szasz, Z. Li, P. Petersson, X.-S. Bai, M. Aldén, D. Lörstad
In press, International Journal of Hydrogen Energy, https://doi.org/10.1016/j.ijhydene.2021.01.087

This paper reports the observations made when operating the CECOST swirl-type gasturbine model combustor with a blend of CH_4 and H_2. The operating range was determined for a range of Reynolds numbers and fuel mixtures. High-speed chemilumninescence imagin and the laser diagnostic techniques PIV and PLIF imaging of OH were performed.

The candidate prepared the operating conditions based on stoichiometric calculations. The laminar flames speed of all investigated fuel mixtures was calculated in Cantera. The candidate took part in the preparation and performance of the experiments, and also did part of the image post-processing of high-speed images. The candidate was involved in the writing and the revision process.

Paper iii: Numeric investigation of the flame stability for lean premixed combustion of hydrogen-enriched methane and syngas in a lab-scale atmospheric swirl burner

M. Bertsch, S. Yu, R.-Z. Szasz, X.-S. Bai, A. A. Subash, M. Aldén
Nordic Flame Days 2019, Turku, Finland

This paper discusses isothermal flow simulations of the CECOST swirl-type burner. LES results for different Reynolds number are compared and the findings of a grid sensitivity study are presented. The performance of a tabulated-chemistry combustion model, the strained FGM model is presented.

The candidate prepared and performed the isothermal LES of the swirl burner, postprocessed the resulting flow field data, prepared the manuscript, and delivered the presentation at the Nordic Flame Days.

Chapter 7

Conclusions and future work

The CECOST swirl burner was investigated for operation with CH_4 and H_2-enriched CH_4. For the future, the further characterisation of the burner with regard to fuel flexibility is the central aim. Experiments with syngas, roughly consisting of equal parts of H_2, CO and CO_2, will be studied.

Another very interesting path to extend the experiments is to study the effect of varying CO_2 dilution on CO/H_2/air combustion in swirl-type flame at atmospheric pressure. The effect of CO_2 dilution on CO/H_2/air combustion in a confined swirl-stabilised flame at atmospheric pressure would be a valuable contribution to the field of research. Flashback and lean blow out limits as a function of dilution would allow valuable new insight.

Yet another plan is to perform simultaneous OH and CH_2O PLIF imaging for a range of fuels, as well as simultaneous OH PLIF and PIV measurements, to increase the understanding of flow-flame interaction in this highly turbulent swirling flame, which would allow validation of combustion models for the numeric study of this burner.

Concerning the simulation of the CECOST swirl burner, this outlook includes the generation of an LES turbulent inflow boundary condition, the preparation of a tabulated chemistry reacting flow solver, for example FGM, that yields accurate results for a wide range of alternative fuels.

Furthermore, the simulation of near flashback and near LBO flames with realistic boundary conditions would represent a unique opportunity to increase the understanding of these processes of the highest industrial relevance, especially complementary to an accompanying in-depth experimental campaign with focus on this topic.

References

[1] P. Weigand et al. “Investigations of swirl flames in a gas turbine model combustor”. In: *Combustion and Flame* 144.1-2 (2006), pp. 205–224. DOI: 10.1016/j.combustflame.2005.07.010.

[2] Qingguo Zhang et al. “Impacts of Hydrogen Addition on Near-Lean Blowout Dynamics in a Swirling Combustor”. In: *Volume 2: Turbo Expo 2007*. ASMEDC, 2007, pp. 189–198. DOI: 10.1115/GT2007-27308.

[3] P. Strakey, T. Sidwell, and J. Ontko. “Investigation of the effects of hydrogen addition on lean extinction in a swirl stabilized combustor”. In: *Proceedings of the Combustion Institute* (2007). DOI: 10.1016/j.proci.2006.07.077.

[4] D. M. Wicksall et al. “The interaction of flame and flow field in a lean premixed swirl-stabilized combustor operated on H2/CH4/air”. In: *Proceedings of the Combustion Institute* (2005). DOI: 10.1016/j.proci.2004.07.021.

[5] O. Tuncer, S. Acharya, and J. H. Uhm. “Dynamics, NOx and flashback characteristics of confined premixed hydrogen-enriched methane flames”. In: *International Journal of Hydrogen Energy* 34.1 (2009), pp. 496–506. DOI: 10.1016/j.ijhydene.2008.09.075.

[6] Nicholas Syred et al. “The effect of hydrogen containing fuel blends upon flashback in swirl burners”. In: *Applied Energy* (2012). DOI: 10.1016/j.apenergy.2011.01.057.

[7] Majid Emadi et al. “Flame structure changes resulting from hydrogen-enrichment and pressurization for low-swirl premixed methane-air flames”. In: *International Journal of Hydrogen Energy* (2012). DOI: 10.1016/j.ijhydene.2012.04.017.

[8] Ali Cemal Benim and Khawar J. Syed. *Flashback Mechanisms in Lean Premixed Gas Turbine Combustion*. 2014. DOI: 10.1016/C2013-0-18847-2.

[9] Tim C. Lieuwen. *Unsteady Combustor Physics*. Cambridge: Cambridge University Press, 2012. DOI: 10.1017/CBO9781139059961.

[10] Won-Wook Kim et al. “Towards Modeling Lean Blow Out in Gas Turbine Flameholder Applications”. In: *Journal of Engineering for Gas Turbines and Power* 128.1 (2006), pp. 40–48. DOI: 10.1115/1.2032450.

[11] Moshe Matalon. “Intrinsic Flame Instabilities in Premixed and Nonpremixed Combustion”. In: *Annual Review of Fluid Mechanics* 39.1 (2007), pp. 163–191. DOI: 10.1146/annurev.fluid.38.050304.092153.

[12] James F. Driscoll. *Turbulent premixed combustion: Flamelet structure and its effect on turbulent burning velocities*. 2008. DOI: 10.1016/j.pecs.2007.04.002.

[13] Santosh J. Shanbhogue, Sajjad Husain, and Tim Lieuwen. “Lean blowoff of bluff body stabilized flames: Scaling and dynamics”. In: *Progress in Energy and Combustion Science* 35.1 (2009), pp. 98–120. DOI: 10.1016/j.pecs.2008.07.003.

[14] M. Stöhr et al. “Dynamics of lean blowout of a swirl-stabilized flame in a gas turbine model combustor”. In: *Proceedings of the Combustion Institute* 33.2 (2011), pp. 2953–2960. DOI: 10.1016/j.proci.2010.06.103.

[15] N. Syred et al. “Effect of inlet and outlet configurations on blow-off and flashback with premixed combustion for methane and a high hydrogen content fuel in a generic swirl burner”. In: *Applied Energy* (2014). DOI: 10.1016/j.apenergy.2013.11.071.

[16] S. Hoffmann, P. Habisreuther, and B. Lenze. “Development and assessment of correlations for predicting stability limits of swirling flames”. In: *Chemical Engineering and Processing: Process Intensification* 33.5 (1994), pp. 393–400. DOI: 10.1016/0255-2701(94)02011-6.

[17] Mohammed Abdulsada et al. “Effect of exhaust confinement and fuel type upon the blowoff limits and fuel switching ability of swirl combustors”. In: *Applied Thermal Engineering* 48 (2012), pp. 426–435. DOI: 10.1016/j.applthermaleng.2012.04.042.

[18] David Page, Brendan Shaffer, and Vincent McDonell. “Establishing operating limits in a commercial lean premixed combustor operating on synthesis gas pertaining to flashback and blowout”. In: *Proceedings of the ASME Turbo Expo*. 2012. DOI: 10.1115/GT2012-69355.

[19] S. Taamallah et al. “Helical vortex core dynamics and flame interaction in turbulent premixed swirl combustion: A combined experimental and large eddy simulation investigation”. In: *Physics of Fluids* 31.2 (2019). DOI: 10.1063/1.5065508.

[20] I. Chterev et al. *Flame and flow topologies in an annular swirling flow*. 2014. DOI: 10.1080/00102202.2014.882916.

[21] Soufien Taamallah, Santosh J. Shanbhogue, and Ahmed F. Ghoniem. "Turbulent flame stabilization modes in premixed swirl combustion: Physical mechanism and Karlovitz number-based criterion". In: *Combustion and Flame* 166 (2016), pp. 19–33. DOI: 10.1016/j.combustflame.2015.12.007.

[22] Yannick Sommerer et al. "Large eddy simulation and experimental study of flashback and blow-off in a lean partially premixed swirled burner". In: *Journal of Turbulence* 5 (2004). DOI: 10.1088/1468-5248/5/1/037.

[23] S. L. Plee and A. M. Mellor. *Review of flashback reported in prevaporizing/premixing combustors*. 1978. DOI: 10.1016/0010-2180(78)90093-7.

[24] Forman A. Williams. *Combustion Theory (2nd Ed.)* 1985. ISBN: 9788578110796.

[25] Tim Lieuwen et al. "Burner Development and Operability Issues Associated with Steady Flowing Syngas Fired Combustors". In: *Combustion Science and Technology* 180.6 (2008), pp. 1169–1192. DOI: 10.1080/00102200801963375.

[26] O. Lucca-Negro and T. O'Doherty. "Vortex breakdown: A review". In: *Progress in Energy and Combustion Science* 27.4 (2001), pp. 431–481. DOI: 10.1016/S0360-1285(00)00022-8.

[27] C. Guin. "Characterization of autoignition and flashback in premixed injection systems". In: *AVT Symp. on Gas Turbine Engine Combustion, Emissions and Alternative Fuels*. 1998.

[28] S. Taamallah et al. "Fuel flexibility, stability and emissions in premixed hydrogen-rich gas turbine combustion: Technology, fundamentals, and numerical simulations". In: *Applied Energy* 154 (2015), pp. 1020–1047. DOI: 10.1016/j.apenergy.2015.04.044.

[29] Kushal S. Kedia and Ahmed F. Ghoniem. "The blow-off mechanism of a bluff-body stabilized laminar premixed flame". In: *Combustion and Flame* (2015). DOI: 10.1016/j.combustflame.2014.10.017.

[30] Nicholas Rock et al. "Near-lean blowoff dynamics in a liquid fueled combustor". In: *Combustion and Flame* (2020). DOI: 10.1016/j.combustflame.2019.10.010.

[31] Anthony J. Morales et al. "Mechanisms of flame extinction and lean blowout of bluff body stabilized flames". In: *Combustion and Flame* (2019). DOI: 10.1016/j.combustflame.2019.02.002.

[32] A. Giusti and E. Mastorakos. "Detailed chemistry LES/CMC simulation of a swirling ethanol spray flame approaching blow-off". In: *Proceedings of the Combustion Institute* (2017). DOI: 10.1016/j.proci.2016.06.035.

[33] Erdzan Hodzic et al. “Large eddy simulation of bluff body flames close to blow-off using an Eulerian stochastic field method”. In: *Combustion and Flame* (2017). DOI: 10.1016/j.combustflame.2017.03.010.

[34] R. W. Schefer, D. M. Wicksall, and Ajay K. Agrawal. “Combustion of hydrogen-enriched methane in a lean premixed swirl-stabilized burner”. In: *Proceedings of the Combustion Institute* (2002).

[35] Qingguo Zhang, David R. Noble, and Tim Lieuwen. “Characterization of Fuel Composition Effects in H2/CO/CH4 Mixtures Upon Lean Blowout”. In: *Journal of Engineering for Gas Turbines and Power* 129.3 (2007), pp. 688–694. DOI: 10.1115/1.2718566.

[36] Gorkem Oztarlik et al. “Suppression of instabilities of swirled premixed flames with minimal secondary hydrogen injection”. In: *Combustion and Flame* (2020). DOI: 10.1016/j.combustflame.2019.12.032.

[37] Xiao Han et al. “Flame interactions in a stratified swirl burner: Flame stabilization, combustion instabilities and beating oscillations”. In: *Combustion and Flame* (2020). DOI: 10.1016/j.combustflame.2019.11.020.

[38] D. G. Pugh et al. “Dissociative influence of H2O vapour/spray on lean blowoff and NOx reduction for heavily carbonaceous syngas swirling flames”. In: *Combustion and Flame* (2017). DOI: 10.1016/j.combustflame.2016.11.010.

[39] A. Amato et al. “Methane oxycombustion for low CO2 cycles: Blowoff measurements and analysis”. In: *Journal of Engineering for Gas Turbines and Power* (2011). DOI: 10.1115/1.4002296.

[40] R. Marsh et al. “Premixed methane oxycombustion in nitrogen and carbon dioxide atmospheres: Measurement of operating limits, flame location and emissions. Proceedings of the Combustion Institute”. In: *Proceedings of the Combustion Institute* (2017). DOI: 10.1016/j.proci.2016.06.057.

[41] Ying Huang and Vigor Yang. “Dynamics and stability of lean-premixed swirl-stabilized combustion”. In: *Progress in Energy and Combustion Science* 35.4 (2009), pp. 293–364. DOI: 10.1016/j.pecs.2009.01.002.

[42] Zhi X. Chen et al. “Large Eddy Simulation of a dual swirl gas turbine combustor: Flame/flow structures and stabilisation under thermoacoustically stable and unstable conditions”. In: *Combustion and Flame* 203 (2019), pp. 279–300. DOI: 10.1016/j.combustflame.2019.02.013.

[43] Timothy C. Williams, Christopher R. Shaddix*, and Robert W. Schefer. “Effect of Syngas Composition and CO 2 -Diluted Oxygen on Performance of a Premixed Swirl-Stabilized Combustor”. In: *Combustion Science and Technology* 180.1 (2007), pp. 64–88. DOI: 10.1080/00102200701487061.

[44] Min Chul Lee et al. “Experimental study on the effect of N 2, CO 2, and steam dilution on the combustion performance of H 2 and CO synthetic gas in an industrial gas turbine”. In: *Fuel* (2012). DOI: 10.1016/j.fuel.2012.05.028.

[45] Graham E. Ballachey and Matthew R. Johnson. “Prediction of blowoff in a fully controllable low-swirl burner burning alternative fuels: Effects of burner geometry, swirl, and fuel composition”. In: *Proceedings of the Combustion Institute* 34.2 (2013), pp. 3193–3201. DOI: 10.1016/j.proci.2012.05.095.

[46] Nor Afzanizam Samiran et al. “Swirl stability and emission characteristics of CO-enriched syngas/air flame in a premixed swirl burner”. In: *Process Safety and Environmental Protection* 112 (2017), pp. 315–326. DOI: 10.1016/j.psep.2017.07.011.

[47] Shaoshuai Li et al. “Investigation of dilution effects on partially premixed swirling syngas flames using a LES-LEM approach”. In: *Journal of the Energy Institute* 91.6 (2018), pp. 902–915. DOI: 10.1016/j.joei.2017.09.005.

[48] W. P. Jones, A. J. Marquis, and V. N. Prasad. “LES of a turbulent premixed swirl burner using the Eulerian stochastic field method”. In: *Combustion and Flame* (2012). DOI: 10.1016/j.combustflame.2012.04.008.

[49] David Butz et al. “Large Eddy Simulations of a turbulent premixed swirl flame using an algebraic scalar dissipation rate closure”. In: *Combustion and Flame* (2015). DOI: 10.1016/j.combustflame.2015.05.003.

[50] Hongda Zhang et al. “Large Eddy Simulation of Turbulent Premixed Swirling Flames Using Dynamic Thickened Flame with Tabulated Detailed Chemistry”. In: *Flow, Turbulence and Combustion* (2017). DOI: 10.1007/s10494-016-9791-9.

[51] K.-J. Nogenmyr et al. “Large eddy simulation and laser diagnostic studies on a low swirl stratified premixed flame”. In: *Combustion and Flame* 156.1 (2009), pp. 25–36. ISSN: 0010-2180. DOI: https://doi.org/10.1016/j.combustflame.2008.06.014. URL: http://www.sciencedirect.com/science/article/pii/S0010218008002083.

[52] K.-J. Nogenmyr et al. “Structure and stabilization mechanism of a stratified premixed low swirl flame”. In: *Proceedings of the Combustion Institute* 33.1 (2011), pp. 1567–1574. ISSN: 1540-7489. DOI: https://doi.org/10.1016/j.proci.2010.06.011. URL: http://www.sciencedirect.com/science/article/pii/S1540748910000155.

[53] Henning Carlsson et al. “Numerical and experimental study of flame propagation and quenching of lean premixed turbulent low swirl flames at different Reynolds numbers”. In: *Combustion and Flame* 162.6 (2015), pp. 2582–2591. ISSN: 0010-2180. DOI: https://doi.org/10.1016/j.combustflame.2015.03.007. URL: http://www.sciencedirect.com/science/article/pii/S0010218015000826.

[54] I. Langella et al. “Large Eddy Simulation of Premixed Combustion: Sensitivity to Subgrid Scale Velocity Modeling”. In: *Combustion Science and Technology* (2017). DOI: 10.1080/00102202.2016.1193496.

[55] Ugo Piomelli. *Wall-layer models for large-eddy simulations*. 2008. DOI: 10.1016/j.paerosci.2008.06.001.

[56] Sanjeeb T. Bose and George Ilhwan Park. *Wall-Modeled Large-Eddy Simulation for Complex Turbulent Flows*. 2018. DOI: 10.1146/annurev-fluid-122316-045241.

[57] G John-Puthenveettil and S Jakirlić. “On “Adaptive Wall-Functions” for LES of Flow and Heat Transfer”. In: *New Results in Numerical and Experimental Fluid Mechanics IX: Contributions to the 18th STAB/DGLR Symposium, Stuttgart, Germany, 2012*. Ed. by Andreas Dillmann et al. Cham: Springer International Publishing, 2014, pp. 103–112. DOI: 10.1007/978-3-319-03158-3_11.

[58] G. Boudier, L. Y.M. Gicquel, and T. J. Poinsot. “Effects of mesh resolution on large eddy simulation of reacting flows in complex geometry combustors”. In: *Combustion and Flame* (2008). DOI: 10.1016/j.combustflame.2008.04.013.

[59] Yacine Addad et al. “Optimal unstructured meshing for large eddy simulations”. In: *ERCOFTAC Series*. 2008. DOI: 10.1007/978-1-4020-8578-9_8.

[60] P. Benard et al. “Large-Eddy Simulation of the lean-premixed PRECCINSTA burner with wall heat loss”. In: *Proceedings of the Combustion Institute* 37.4 (2019), pp. 5233–5243. DOI: 10.1016/j.proci.2018.07.026.

[61] I. B. Celik, Z. N. Cehreli, and I. Yavuz. “Index of resolution quality for large eddy simulations”. In: *Journal of Fluids Engineering, Transactions of the ASME*. 2005. DOI: 10.1115/1.1990201.

[62] Simon E. Gant. “Reliability issues of LES-related approaches in an industrial context”. In: *Flow, Turbulence and Combustion* (2010). DOI: 10.1007/s10494-009-9237-8.

[63] Yang Zhiyin. *Large-eddy simulation: Past, present and the future*. 2015. DOI: 10.1016/j.cja.2014.12.007.

[64] Nitin S. Dhamankar, Gregory A. Blaisdell, and Anastasios S. Lyrintzis. "Overview of turbulent inflow boundary conditions for large-eddy simulations". In: *AIAA Journal* 56.4 (2018), pp. 1317–1334. DOI: 10.2514/1.J055528.

[65] G. R. Tabor and M. H. Baba-Ahmadi. *Inlet conditions for large eddy simulation: A review*. 2010. DOI: 10.1016/j.compfluid.2009.10.007.

[66] Soufien Taamallah et al. "On the characteristic flow and flame times for scaling oxy and air flame stabilization modes in premixed swirl combustion". In: *Proceedings of the Combustion Institute* 36.3 (2017), pp. 3799–3807. DOI: 10.1016/j.proci.2016.07.022.

[67] Peter Weigand et al. "Experimental investigations of an oscillating lean premixed CH4/air swirl flame in a gas turbine model combustor". In: 2005. URL: https://elib.dlr.de/3418/.

[68] Seyed Mohammad Hosseini et al. "Study of Flame Dynamics and Flashback Mechanism in a Gas Turbine Combustor Using Simultaneous OH-PLIF and PIV". In: *46th AIAA/ASME/SAE/ASEE Joint Propulsion Conference & Exhibit*. Reston, Virigina: American Institute of Aeronautics and Astronautics, 2010. DOI: 10.2514/6.2010-6668.

[69] Yunzhe Zheng et al. "Large-eddy simulation of mixing and combustion in a premixed swirling combustor with synthesis gases". In: *Computers and Fluids* 88 (2013), pp. 702–714. DOI: 10.1016/j.compfluid.2013.04.003.

[70] Hosein Foroutan and Savas Yavuzkurt. "International Journal of Heat and Fluid Flow A partially-averaged Navier – Stokes model for the simulation of turbulent swirling flow with vortex breakdown". In: *International Journal of Heat and Fluid Flow* 50 (2014), pp. 402–416. DOI: 10.1016/j.ijheatfluidflow.2014.10.005.

[71] D. Noh et al. "Azimuthally-driven subharmonic thermoacoustic instabilities in a swirl-stabilised combustor". In: *Proceedings of the Combustion Institute* (2019). DOI: 10.1016/j.proci.2018.07.090.

[72] S. Hermeth et al. "LES evaluation of the effects of equivalence ratio fluctuations on the dynamic flame response in a real gas turbine combustion chamber". In: *Proceedings of the Combustion Institute* (2013). DOI: 10.1016/j.proci.2012.07.013.

[73] P. Weigand et al. "Investigations of swirl flames in a gas turbine model combustor: I. Flow field, structures, temperature, and species distributions". In: *Combustion and Flame* 144.1-2 (2006), pp. 205–224. DOI: 10.1016/j.combustflame.2005.07.010.

[74] A. Widenhorn et al. “Numerical Characterization of the Non-Reacting Flow in a Swirled Gasturbine Model Combustor”. In: *High Performance Computing in Science and Engineering ‘07*. Berlin, Heidelberg: Springer Berlin Heidelberg, 2008, pp. 431–444. DOI: 10.1007/978-3-540-74739-0_29.

[75] Axel Widenhorn, Berthold Noll, and Manfred Aigner. “Numerical Study of a Non-Reacting Turbulent Flow in a Gas-turbine Model Combustor”. In: *47th AIAA Aerospace Sciences Meeting including The New Horizons Forum and Aerospace Exposition*. January. Orlando, Florida: American Institute of Aeronautics and Astronautics, 2009, pp. 1–17. DOI: 10.2514/6.2009-647.

[76] A. C. Benim et al. “Analysis of Turbulent Swirling Flow in an Isothermal Gas Turbine Combustor Model”. In: *Volume 4A: Combustion, Fuels and Emissions*. Vol. 4A. American Society of Mechanical Engineers, 2014, pp. 1–10. DOI: 10.1115/GT2014-25008.

[77] Zhi X. Chen et al. “Interaction between self-excited oscillations and fuel-air mixing in a dual swirl combustor”. In: *Proceedings of the Combustion Institute* (2019). DOI: 10.1016/j.proci.2018.08.042.

[78] G. Lartigue, U. Meier, and C. Bérat. “Experimental and numerical investigation of self-excited combustion oscillations in a scaled gas turbine combustor”. In: *Applied Thermal Engineering* 24.11-12 (2004), pp. 1583–1592. DOI: 10.1016/j.applthermaleng.2003.10.026.

[79] S. Roux et al. “Studies of mean and unsteady flow in a swirled combustor using experiments, acoustic analysis, and large eddy simulations”. In: *Combustion and Flame* 141.1-2 (2005), pp. 40–54. DOI: 10.1016/j.combustflame.2004.12.007.

[80] Guillaume Daviller et al. “A Mesh Adaptation Strategy to Predict Pressure Losses in LES of Swirled Flows”. In: *Flow, Turbulence and Combustion* 99.1 (2017), pp. 93–118. DOI: 10.1007/s10494-017-9808-z.

[81] Erdzan Hodzic et al. “Numerical and Experimental Investigation of the CeCOST Swirl Burner”. In: *Proceedings of ASME Turbo Expo 2018: Turbomachinery Technical Conference and Exposition* (2018), pp. 1–12. DOI: 10.1115/GT201875760.

[82] E. M. Laws and J. L. Livesey. “FLOW THROUGH SCREENS.” In: *Annu Rev Fluid Mech* (1978). DOI: 10.1146/annurev.fl.10.010178.001335.

[83] Johan Groth and Arne V. Johansson. “Turbulence reduction by screens”. In: *Journal of Fluid Mechanics* (1988). DOI: 10.1017/S0022112088003209.

[84] *Engineering ToolBox, (2001)*. URL: https://www.engineeringtoolbox.com (visited on 12/09/2020).

[85] Arman Ahamed Subash. “Laser-Based Investigations of Combustion Phenomena in Gas Turbine Related Burners”. PhD. Lund University, 2018. ISBN: 978-91-7753-523-2.

[86] *OpenFOAM v6*. URL: https://openfoam.org/version/6/.

[87] Horn Jiunn Sheen et al. “Correlation of Swirl Number for a Radial-Type Swirl Generator”. In: *Experimental Thermal and Fluid Science* (1996). DOI: 10.1016/0894-1777(95)00135-2.

[88] David G. Goodwin. “CANTERA: An open-source, object-oriented software suite for combustion”. In: *NSF Workshop on Cyber-based Combustion Science*. 2006. URL: http://www.cantera.org.

[89] Gregory P. Smith et al. *GRI-MECH 3.0*. URL: http://www.me.berkeley.edu/gri%7B%5C_%7Dmech/.